Spin coating and air-jet blowing of thin viscous drops

I. S. McKinley, S. K. Wilson and B. R. Duffy

Department of Mathematics, University of Strathclyde,

Livingstone Tower, 26 Richmond Street,

Glasgow G1 1XH, United Kingdom.

(July 13, 1998)

Abstract

Using the lubrication approximation we investigate the spreading of a finite-sized thin drop of incompressible Newtonian fluid on a planar substrate subjected to a jet of air blowing normally to the substrate. Three specific problems are studied in detail: a jet of air acting normally to the substrate when gravity effects are negligible, a jet of air directed vertically downwards onto a sessile drop on a horizontal substrate and a jet of air directed vertically upwards onto a pendent drop on a horizontal substrate. The dynamics of the moving contact line are modelled by means of a generalised "Tanner Law" relating the contact angle to the speed of the contact line. Both symmetric two-dimensional and axisymmetric three-dimensional geometries are considered; the latter case is equivalent to that of an axisymmetric drop spreading on a turntable rotating at constant angular velocity (the simplest model for spin coating). Quasi-static solutions for the drop profile are obtained in the limit of small capillary number and the stability of equilibrium solutions to small perturbations is determined. The analysis is then extended to include drops with a dry patch at their centre which are found to be unconditionally unstable in all the cases investigated.

I. INTRODUCTION

Applying a thin film of fluid to a solid substrate is an industrial problem of great practical importance, making it necessary that the dynamics of the different coating processes are understood as fully as possible. Amongst these processes are spin coating (in which the fluid is placed onto a rotating substrate and spreads out under the action of the centrifugal force), and blowing a jet of air onto a fluid on a stationary substrate (hereafter referred to simply as "air-jet blowing").

One of the first analyses of spin coating was performed by Emslie *et al.*[1], who considered the evolution of a thin axisymmetric film of viscous Newtonian fluid on a substrate rotating with constant angular velocity. They obtained the exact solution for the evolution of the free-surface profile due to purely centrifugal and viscous shear forces and showed that initially non-uniform profiles tend to become increasingly uniform during spinning. This pioneering work has been the basis for many subsequent investigations of spin coating. For example, Yanagisawa[2] and Tu[3] analysed the effect of different slip models at the solid/fluid interface, Acrivos *et al.*[4], Lawrence[5] and Lawrence and Zhou[6] investigated the spin coating of non-Newtonian fluids, while Jenekhe and Schuldt[7] and Burgess and Wilson[8] investigated the spin coating of Bingham materials. Other authors have analysed a variety of additional physical effects on the spin coating of a uniform film, including Meyerhofer[9], who included evaporation from the film, Higgins[10], who included fluid inertia, Bornside *et al.*[11], who included the effects of variations in concentration, viscosity and diffusivity across the film, and Reisfeld *et al.*[12], who included evaporation and absorption effects.

By performing the analysis suggested by Troian *et al.*[13], Moriarty *et al.*[14] solved the unsteady spin-coating problem both numerically and asymptotically in the limit of weak surface tension (in which surface tension effects are significant only in an "inner" region near the edge of the drop). Troian *et al.*[13] performed a linear stability analysis of the quasi-static solution in the inner region which they found to be always unstable to sufficiently long-wavelength azimuthal disturbances. Fraysse and Homsy[15] found that their experimentally-

measured values for the azimuthal wavenumber and growth rate of the observed "fingering" instability were in good agreement with Troian *et al.*'s[13] analytical predictions, provided that the experimentally-measured values of the critical radius of the drop at the onset of instability were used.

Moriarty *et al.*[14] also considered the two-dimensional problem of a drop spreading on a horizontal substrate under the action of a jet of air blowing either vertically downwards onto the substrate or parallel to it. Again the resulting unsteady problem was solved numerically and asymptotically in the limit of weak surface tension. In the first case, the jet was modelled simply as a parabolic pressure distribution in the air, and the shear stress at the free surface of the fluid caused by the air flow was neglected, while in the second case the jet was modelled as a constant shear stress distribution at the free surface of the fluid while the variations in the air pressure were neglected. Similar simplified models for the effect of a jet of air on a thin fluid film have also been used to study the closely related "air knife" process, in which the thickness of the fluid film coated onto a moving substrate is controlled by varying the strength of a jet of air directed onto the fluid (see, for example, the theoretical studies of Ellen and Tu[16] and Tuck and Vanden Broeck[17] and the experimental study by Buchlin *et al.*[18]).

In the present work we shall focus on the interesting behaviour found in both spin-coating and air-jet-blowing problems due to the presence of both surface tension and moving-contact-line effects. The motion of contact lines has been the subject of much debate in recent years (see, for example, the work by Hocking[19]). The key issue is the determination of the relationship between the experimentally-measured macroscopic contact angle θ (inferred from global properties or measured some distance from the contact line) and the speed of the contact line U. One approach takes the view that it is not necessary to model the details of the flow in the vicinity of the contact line, but that one may instead adopt an empirically-determined "Tanner Law" relating U and θ. Greenspan[20] pioneered this approach by proposing a linear relationship, and this was subsequently generalised to a power-law dependence by Ehrhard and Davis[21], who found that a particular cubic power law

gave the best fit to their experimental data. This approach has the great practical advantage that the difficult problem of the flow in the vicinity of the contact line is circumvented, and as a result it has been widely used in recent years to study several problems involving the dynamics of thin fluid films. For example, it was used by Greenspan[20] to study the spreading of a drop, by Ehrhard and Davis[21] to study the spreading of a non-isothermal drop, by Ehrhard[22] to study the spreading of a pendent drop, by Braun *et al.*[23] to study the reactive spreading of a drop, by Wilson and Terrill[24] and López *et al.*[25] to study the opening and closing of a hole in a fluid film, by López *et al.*[26] to study the non-isothermal draining of a fluid film down an inclined plane, by López *et al.*[27] to study the effect of fluid inertia on the draining of a fluid film down an inclined plane and by Wilson and Duffy[28] to study the quasi-static stability of a rivulet draining down a non-uniform substrate. An alternative approach takes the view that, while the former approach may yield physically-reasonable results for relatively little effort, it is conceptually superior to determine the relationship between U and θ analytically rather than impose it (rather like an additional "constitutive law"). In order to perform this kind of calculation some additional physical effects must be included, but there is currently no agreement on what effects are appropriate. Hocking[29,30] has determined the relationship between U and θ under the assumptions of a fixed microscopic contact angle and a simple slip model at the substrate, while more recently Hocking[31] included intermolecular forces. On the other hand, Shikhmurzaev[32,33] modelled the thermodynamic state of the interfacial regions near the contact line, allowing for relaxation in properties of a fluid element as it traverses the contact-line zone. He derived the relationship between θ and U predicted by the model and also showed that the model resolves the stress singularity at a moving contact line. In particular, Shikhmurzaev[33] obtained numerically-calculated examples of non-thin drops spreading on a substrate due to gravity and to rotation of the substrate. For simplicity we shall adopt the first approach in the present work, but shall employ a rather general Tanner Law relating U and θ which incorporates as special cases all the specific forms used by earlier authors.

In this paper we investigate the quasi-static spreading of a finite-sized thin drop of

incompressible, Newtonian viscous fluid attached to a planar substrate in the presence of a jet of air in both symmetric planar two-dimensional and axisymmetric three-dimensional geometries. Since we shall consider only the leading-order solution in the quasi-static limit the stress singularity at the moving contact line does not appear explicitly in the present work (although, as Hocking[19] has shown, it would do so if we continued the analysis to higher orders). Three specific problems are studied in detail: a jet of air acting normally to the substrate when gravity effects are negligible, a jet of air directed vertically downwards onto a sessile drop on a horizontal substrate and a jet of air directed vertically upwards onto a pendent drop on a horizontal substrate. Both "annular" and "non-annular" geometries will be considered (see Sec. VII A for a definition of these terms). Since, for the simple model of the jet we shall adopt, the axisymmetric air-jet-blowing problem is identical to the axisymmetric spin-coating problem of a drop of fluid attached to a horizontal substrate rotating with uniform angular velocity, the results in the axisymmetric case will also apply to the spin-coating problem with an appropriate redefinition of the parameters. For each problem we determine the physically-realisable equilibrium solutions for the profile of the drop and investigate their stability to uniform perturbations in the two-dimensional case and axisymmetric perturbations in the three-dimensional case. Note that the restricted class of perturbations considered here does not include the (non-uniform and non-axisymmetric) fingering instabilities mentioned earlier.

II. PROBLEM FORMULATION

Consider a constant volume of incompressible Newtonian fluid with constant viscosity μ, density ρ and surface tension σ spreading on a solid horizontal planar substrate in the presence of a jet of air. We analyse both the symmetric planar two-dimensional case, denoted by (p), and the axisymmetric three-dimensional case, denoted by (a), for which we employ Cartesian coordinates (x, z) and cylindrical polar coordinates (r, z) respectively, with the z-axis vertically upwards or downwards as appropriate. The thickness of the fluid film is

denoted by $z = h(x,t)$ (p) or $z = h(r,t)$ (a), where t denotes time, and the velocity of the fluid is denoted by $\mathbf{u} = \mathbf{u}(x,z,t)$ (p) or $\mathbf{u} = \mathbf{u}(r,z,t)$ (a). Following Moriarty *et al.*[14] we model the jet of air as a parabolic pressure distribution in the air so that $p = p_0 - kx^2/2$ (p) or $p = p_0 - kr^2/2$ (a), where p denotes the pressure, p_0 is the maximum value of the air pressure at the centre of the drop and k is a positive constant; the shear stress at the free surface of the fluid caused by the air flow is assumed to be negligible. The geometry of the problem in the case of a sessile drop is shown in Fig. 1; the only difference in the pendent case is that the direction of gravity is reversed.

We assume that the speed of the contact line, at position $x = R(t)$ (p) or $r = R(t)$ (a), is related to the contact angle $\theta = \theta(t)$ by the general Tanner Law

$$R_t = \kappa F\left(\frac{\theta}{\theta_0}\right), \tag{1}$$

where κ is an empirically-determined positive constant with dimensions of velocity, $F(\theta/\theta_0)$ is an empirically-determined function satisfying $F(1) = 0$, and $\theta_0 > 0$ is the equilibrium contact angle. Typically $F(\theta/\theta_0)$ is a monotonically-increasing function and so its first non-zero derivative at $\theta = \theta_0$ will be positive and of odd order.

Provided that inertia effects are negligible (i.e. provided that the appropriate Reynolds number is sufficiently small) and the drop sufficiently thin, the conventional lubrication approximation to the governing Navier-Stokes equations yields

$$p_z = -\rho g, \tag{2}$$

$$\begin{cases} \mu u_{zz} = p_x, & (p) \\ \mu u_{zz} = p_r, & (a) \end{cases} \tag{3}$$

$$\begin{cases} u_x + w_z = 0, & (p) \\ \dfrac{1}{r}(ru)_r + w_z = 0, & (a) \end{cases} \tag{4}$$

where g denotes acceleration due to gravity, subject to the boundary conditions

$$u = 0 \quad \text{on} \quad z = 0, \tag{5}$$

$$\mu u_z = 0 \quad \text{on} \quad z = h, \tag{6}$$

$$\begin{cases} p = p_0 - \dfrac{kx^2}{2} - \sigma h_{xx} & (p) \\ p = p_0 - \dfrac{kr^2}{2} - \dfrac{\sigma}{r}(rh_r)_r & (a) \end{cases} \quad \text{on} \quad z = h, \tag{7}$$

$$\begin{cases} w = h_t + uh_x & (p) \\ w = h_t + uh_r & (a) \end{cases} \quad \text{on} \quad z = h, \tag{8}$$

where the fluid velocity has been written $\mathbf{u}=(u, w)$ in the appropriate coordinates. Equation (5) is the no-slip condition at the substrate, Eq. (6) represents zero tangential stress at the free surface and Eq. (7) is the normal stress condition which includes both the effects of surface tension and the non-uniform external pressure loading caused by the jet of air. Equation (8) is the kinematic free-surface condition which can be re-written in the form

$$\begin{cases} h_t + Q_x = 0, & (p) \\ h_t + \dfrac{1}{r}(rQ)_r = 0, & (a) \end{cases} \tag{9}$$

where Q denotes the flux per unit length (p) or circumference (a), defined by

$$Q = \int_0^h u \, \mathrm{d}z. \tag{10}$$

Solving Eqs. (2) – (7) for u allows Q to be evaluated from Eq. (10) and substituting Q into Eq. (9) gives the governing equation for h.

We non-dimensionalise the problem using a characteristic horizontal length scale L (to be defined subsequently) and κ as the characteristic horizontal velocity scale. The corresponding non-dimensional variables are defined by $x = Lx'$, $r = Lr'$, $R = LR'$, $h = \theta_0 Lh'$, $t = Lt'/\kappa$ and $\theta = \theta_0\theta'$. Dropping the primes at once for simplicity we obtain the non-dimensional version of the governing equation, namely

$$\begin{cases} Ch_t + \left[\dfrac{h^3}{3}\left((h_{xx} - G^2 h)_x + Jx\right)\right]_x = 0, & (p) \\ Ch_t + \dfrac{1}{r}\left[\dfrac{rh^3}{3}\left\{\left(\dfrac{1}{r}(rh_r)_r - G^2 h\right)_r + Jr\right\}\right]_r = 0, & (a) \end{cases} \tag{11}$$

together with the non-dimensional version of Eq. (1), namely

$$R_t = F(\theta), \tag{12}$$

where the constant $J = kL^3/\sigma\theta_0$ is a non-dimensional measure of the jet strength, $C = \kappa\mu/\sigma\theta_0^3$ is the capillary number and $G^2 = \rho g L^2/\sigma$ is the Bond number. The appropriate boundary conditions for Eq. (11) are

$$h(R,t) = 0, \tag{13}$$

$$\begin{cases} h_x(R,t) = -\theta, & (p) \\ h_r(R,t) = -\theta, & (a) \end{cases} \tag{14}$$

together with the regularity conditions

$$\begin{cases} h_x(0,t) = 0, & (p) \\ h_r(0,t) = 0, & (a) \end{cases} \tag{15}$$

$$Q(0,t) = 0, \tag{16}$$

which must be satisfied together with appropriate initial conditions for h and R. The volume of the drop is given by

$$\begin{cases} 2V = 2\displaystyle\int_0^R h \,\mathrm{d}x, & (p) \\ 2\pi V = 2\pi \displaystyle\int_0^R hr \,\mathrm{d}r. & (a) \end{cases} \tag{17}$$

Note that if we identify the dimensional jet strength k with $\rho\omega^2$ then Eq. (11)(a) is exactly the same as the corresponding equation obtained in the special case $G = 0$ by Moriarty *et al.*[14] (their Eq. 30) for a thin axisymmetric fluid film spreading under the action of the centrifugal force on a substrate rotating uniformly with angular speed ω. Hence all our results for the axisymmetric air-jet-blowing problem also apply to the axisymmetric spin-coating problem. We note, however, that as Emslie *et al.*[1] pointed out, in this problem the Coriolis force can be properly neglected compared to the centrifugal force (as it was by Emslie *et al.*[1] and Moriarty *et al.*[14]) only if the fluid motion is sufficiently slow.

III. QUASI-STATIC MOTION

In the limit of small capillary number, $C \to 0$, the contact line moves slowly relative to the bulk of the fluid and so the dynamics of the motion are controlled by those of the contact line. At leading order in $C \ll 1$ we drop the unsteady term in Eq. (11) and so the flux is constant; then by Eq. (16) it is zero everywhere. Hence we obtain a third-order ordinary differential equation for the thickness of the drop:

$$\begin{cases} (h_{xx} - G^2 h)_x + Jx = 0, & (p) \\ \left(h_{rr} + \dfrac{h_r}{r} - G^2 h\right)_r + Jr = 0, & (a) \end{cases} \tag{18}$$

to be integrated subject to Eqs. (13), (14) and (15). The solution for h is easily obtained and can be written in the form

$$h = \theta f(\cdot, R) + J g(\cdot, R), \tag{19}$$

where the symbol "$\cdot$" denotes x (p) or r (a) and the functions $f(\cdot, R)$ and $g(\cdot, R)$ are given by

$$\begin{cases} f(x, R) = \dfrac{\cosh GR - \cosh Gx}{G \sinh GR}, & (p) \\ f(r, R) = \dfrac{I_0(GR) - I_0(Gr)}{G I_1(GR)}, & (a) \end{cases} \tag{20}$$

$$\begin{cases} g(x, R) = \dfrac{2R(\cosh GR - \cosh Gx) + G \sinh GR(x^2 - R^2)}{2G^3 \sinh GR}, & (p) \\ g(r, R) = \dfrac{2R(I_0(GR) - I_0(Gr)) + G I_1(GR)(r^2 - R^2)}{2G^3 I_1(GR)}, & (a) \end{cases} \tag{21}$$

where $I_0(\cdot)$ and $I_1(\cdot)$ are modified Bessel functions of the first kind. The volume of this quasi-equilibrium drop is given by

$$V = \theta S(R) + J T(R), \tag{22}$$

where the functions $S = S(R)$ and $T = T(R)$ are given by

$$S(R) = \begin{cases} \dfrac{GR \cosh GR - \sinh GR}{G^2 \sinh GR}, & (p) \\ \dfrac{GR^2 I_0(GR) - 2R I_1(GR)}{2G^2 I_1(GR)}, & (a) \end{cases} \tag{23}$$

$$T(R) = \begin{cases} \dfrac{3GR^2\cosh GR - 3R\sinh GR - G^2R^3\sinh GR}{3G^4\sinh GR}, & (p) \\ \dfrac{4GR^3I_0(GR) - 8R^2I_1(GR) - G^2R^4I_1(GR)}{8G^4I_1(GR)}. & (a) \end{cases} \tag{24}$$

Note that the functions $f(\cdot, R)$ and $S(R)$ are precisely the familiar expressions for h and V in the absence of blowing ($J = 0$).

When $g \neq 0$ we can, without loss of generality, choose the horizontal lengthscale L to be the capillary length $(\sigma/\rho g)^{1/2}$ (corresponding to setting $|G| = 1$). Alternatively, whatever the value of g, we can (again without loss of generality) choose either $L = (\sigma\theta_0/k)^{1/3}$ (corresponding to setting $J = 1$), or $L = (V/\theta_0)^{1/2}$ (p), $L = (V/\theta_0)^{1/3}$ (a) (corresponding to setting $V = 1$). Of course all of these choices are equally valid; however in order to treat clearly both the problem of a drop with fixed volume under a jet of varying strength and the problem of a drop of variable volume under a jet of fixed strength we need to retain both the parameters V and J explicitly in what follows. We therefore choose L to be the capillary length, and so the sessile ($g > 0$) and pendent ($g < 0$) cases correspond to $G = 1$ and $G = i$ respectively. The special case of zero gravity corresponds to the limit $G \to 0$, and in this case L remains arbitrary.

Rearranging Eq. (22) we obtain an expression for the contact angle θ for constant $V = V_0$ and $J = J_0$:

$$\theta = \frac{V_0 - J_0T(R)}{S(R)}. \tag{25}$$

Substituting this expression for θ into Eq. (12) we obtain a non-linear first-order differential equation for the speed of the contact line, namely

$$R_t = F\left(\frac{V_0 - J_0T(R)}{S(R)}\right), \tag{26}$$

to be solved subject to an appropriate initial condition on $R(t)$.

IV. EQUILIBRIUM SOLUTIONS

In equilibrium $\theta = 1$ and $R = R^0$, say. Using Eq. (22) we can either write the volume $V = V(R^0)$ as a function of R^0 for fixed $J = J_0$ in the form

$$V(R^0) = S(R^0) + J_0 T(R^0), \tag{27}$$

or write the jet strength $J = J(R^0)$ as a function of R^0 for fixed $V = V_0$ in the form

$$J(R^0) = \frac{V_0 - S(R^0)}{T(R^0)}. \tag{28}$$

The possible equilibrium positions of the contact line $R = R^0$ are the solutions of $V = V_0$ for $J = J_0$ (where $V_0 > 0$ and $J_0 > 0$ are prescribed constants) and so R^0 satisfies

$$V_0 = S(R^0) + J_0 T(R^0). \tag{29}$$

V. STABILITY ANALYSIS

To determine the stability of an equilibrium drop of radius $R = R^0$ to small uniform (p) or axisymmetric (a) perturbations we write $R(t) = R^0 + R^1(t)$ and expand Eq. (26) for small R^1 to yield

$$(R^1)_t = \frac{M(\lambda R^1)^m}{m!}, \tag{30}$$

where $M = \mathrm{d}^m F(\theta)/\mathrm{d}\theta^m|_{\theta=1} > 0$ $(m = 1, 3, 5, \ldots)$ is the first non-zero derivative of $F(\theta)$ evaluated at $\theta = 1$ and λ is a constant given by

$$\lambda = -\frac{S'(R^0) + J_0 T'(R^0)}{S(R^0)}. \tag{31}$$

Equation (30) is easily solved to yield

$$R^1 = \begin{cases} \bar{R} e^{\lambda M t} & \text{if } m = 1, \\ \bar{R}\left(1 - \dfrac{(m-1)M(\lambda\bar{R})^m t}{\bar{R} m!}\right)^{-\frac{1}{m-1}} & \text{if } m = 3, 5, 7, \ldots, \end{cases} \tag{32}$$

where $\bar{R} = R^1(0)$ is the initial perturbation to the radius of the drop. Equation (32) shows that an equilibrium drop is unstable to small perturbations when $\lambda > 0$ and stable when $\lambda < 0$. Small perturbations grow or decay exponentially when $m = 1$ and algebraically when $m = 3, 5, 7, \ldots$. Examining Eq. (31) shows that for marginal stability we require

$$\frac{V'(R^0)}{S(R^0)} = 0, \tag{33}$$

where $V(R^0)$ is given by Eq. (27), or alternatively, we can write Eq. (33) in the equivalent form

$$\frac{J'(R^0)T(R^0)}{S(R^0)} = 0, \tag{34}$$

where $J(R^0)$ is given by Eq. (28).

Hereafter, we drop the zero superscript on R for clarity.

VI. RESULTS

A. Explanation of figures

In what follows we present results for both the problem of a drop with fixed volume under a jet of varying strength (that is, variable J and fixed V) and the problem of a drop of variable volume under a jet of fixed strength (that is, variable V and fixed J) for both sessile and pendent drops and in the special case of zero gravity. Since the results for the planar case are qualitatively similar to the axisymmetric case we present the plots for the latter case only, although relevant results for the planar case are given where appropriate for completeness.

Figure 2 shows plots of J against R for three values of V_0 in the zero-gravity case, and corresponding typical drop profiles are shown in Fig. 3. Figure 4 shows plots of V against R for three values of J_0 in the zero-gravity case; the drop profiles shown in Fig. 3 are again typical. Figure 5 shows an example of the contact angle θ plotted against radius R in the zero-gravity case. Figure 6 shows corresponding examples of the evolution of the radius R as

a function of time t for a particular choice of $F(\theta)$, while Figs. 7 and 8 show corresponding examples of the evolution of the profile of the drop. Figures 9 and 10 show plots of J against R and V against R respectively in the case of a sessile drop, and the corresponding results in the pendent case are given in Figs. 11 and 12. Results for the pendent case corresponding to Figs. 5–8 in the zero-gravity case are given in Figs. 13–16. Finally, Fig. 17 shows an example of the contact angle θ plotted against radius R in the pendent case for a special value of J.

Since we are concerned only with $V > 0$, $J > 0$ and $R > 0$, all the plots of V against R and J against R are restricted to the first quadrant. On these figures the possible equilibrium solutions are classified as either physically-realisable or not physically-realisable (the latter implying that $h < 0$ at some part of the drop) and either stable ($\lambda < 0$) or unstable ($\lambda > 0$). This classification is indicated as follows:

- a solid thick line indicates stable and physical drop profiles,
- a solid thin line indicates stable but unphysical drop profiles,
- a dashed thick line indicates physical but unstable drop profiles,
- a dashed thin line indicates drop profiles that are both unstable and unphysical.

B. Zero-gravity case ($G = 0$)

In the special case of no air jet, $J = 0$, the function V is monotonically increasing in R, and for all values of $V > 0$ there is a single stable and physical equilibrium solution.

Figure 2 shows J plotted against R for $V_0 = 1, 2$ and 3. Each curve has one zero at $R = (3V_0)^{1/2}$ (p) or $R = (8V_0)^{1/3}$ (a), and a maximum $J = J_\mathrm{m}$ at $R = R_\mathrm{m}$, where $J_\mathrm{m} = 6/(5V_0)^{3/2}$ and $R_\mathrm{m} = (5V_0)^{1/2}$ (p) or $J_\mathrm{m} = 3/(4V_0)$ and $R_\mathrm{m} = (16V_0)^{1/3}$ (a). For all values of V_0 we find that $J \to 0$ like $15/R^3$ (p) or $24/R^3$ (a) as $R \to \infty$. The left-hand part of each curve corresponds to stable and physical drop profiles like those numbered 1 and 2 in Fig. 3. At $R = R_\mathrm{m}$ the solutions remain physical and look like profile 3 in Fig. 3 but become unstable. For $R > R_\mathrm{m}$ the equilibrium solutions remain unstable and, as R

increases, eventually become unphysical via $h = 0$ at the origin like profile 4 in Fig. 3, at $R = (15V_0)^{1/2}$, $J = 12/(15V_0)^{3/2}$ (p) or $R = (24V_0)^{1/3}$, $J = 2/(3V_0)$ (a). In the planar case the drop profile changes from having one turning point to three (that is, changes from one like profile 1 to one like profile 2 in Fig. 3) when R increases through $R = R_{\rm m}$, while in the axisymmetric case this change occurs inside the interval of stable and physical drop profiles at $R = (12V_0)^{1/3} < R_{\rm m}$, $J = 2/(3V_0)$. The width of the interval of R values corresponding to stable and physical profiles increases as V_0 is increased, and for any value of J in the range $0 \leq J \leq J_{\rm m}$ there exists a unique stable and physical equilibrium solution; however, $J_{\rm m}$ decreases with increasing V_0.

Figure 4 shows V plotted against R for $J_0 = 1, 2$ and 3, which can be interpreted in a similar way to Fig. 2. Each curve has two zeros, at $R = 0$ and $R = (15/J_0)^{1/3}$ (p) or $R = (24/J_0)^{1/3}$ (a), and a maximum $V = V_{\rm m}$ at $R = R_{\rm m}$, where $V_{\rm m} = (6/J_0)^{2/3}/5$ and $R_{\rm m} = (6/J_0)^{1/3}$ (p) or $V_{\rm m} = 3/(4J_0)$ and $R_{\rm m} = (12/J_0)^{1/3}$ (a). For all values of J_0, we find that $V \to 0$ like $R^2/3$ (p) or $R^3/8$ (a) as $R \to 0$. Again the left-hand part of each curve corresponds to stable and physical drop profiles. At $R = R_{\rm m}$ the solutions remain physical but become unstable, while for $R > R_m$ the equilibrium solutions remain unstable and, as R increases, eventually become unphysical via $h = 0$ at the origin at $R = (12/J_0)^{1/3}$, $V = (12/J_0)^{2/3}/15$ (p) or $R = (16/J_0)^{1/3}$, $V = 2/(3J_0)$ (a). In the planar case the drop profile changes from having one turning point to three when R increases through $R = R_{\rm m}$, while in the axisymmetric case this change occurs inside the interval of stable and physical drop profiles at $R = (8/J_0)^{1/3} < R_{\rm m}$, $V = 2/(3J_0)$. In this case the width of the interval of R values corresponding to stable and physical profiles decreases as J_0 is increased, and for any value of V in the range $0 < V \leq V_{\rm m}$ there exists a unique stable and physical equilibrium solution; however, $V_{\rm m}$ decreases for increasing J_0.

Figure 5 plots contact angle θ, given by Eq. (25), against radius R in the case $V_0 = 0.4$ and $J_0 = 1$. The thick line corresponds to physical solutions and the thin line corresponds to unphysical solutions. The points of intersection with the horizontal line $\theta = 1$ correspond to equilibrium solutions at $R \approx 1.5608$ (stable) and $R \approx 2.7233$ (unstable). Figure 6 plots

examples of the evolution of the radius R as a function of time t obtained by numerically solving Eq. (26) in the particular case $F(\theta) = \theta^3 - 1$. Detailed analysis in the vicinity of the contact line (see, for example, Hocking[19], Oron *et al.*[34] and Duffy and Wilson[35]) motivates this specific choice of Tanner Law. The shaded area denotes a region of unphysical solutions; our computations exclude this region. Evidently for all the initial conditions shown in Fig. 6 the drop evolves to the stable equilibrium solution with $R \approx 1.5608$. Figs. 7 and 8 show the evolution of the drop profile in the cases $R(0) = 0.5$ and $R(0) = 2.3$ respectively; in both figures the stable equilibrium solution with $R \approx 1.5608$ is shown with a dashed curve. (Note that Figs. 7 and 8 use different vertical scales, for clarity.)

C. Sessile case ($G = 1$)

In the special case $J = 0$ the function V is monotonically increasing in R and for all values of $V > 0$ there is a single stable and physical equilibrium solution, just as in the zero-gravity case.

Figures 9 and 10 show J plotted against R for $V_0 = 1, 2$ and 3 and V plotted against R for $J_0 = 1, 2$ and 3. The qualitative behaviour of the solutions in this case is the same as that of the zero-gravity solutions and so, for the sake of brevity, the details are not repeated here.

D. Pendent case ($G = i$)

In the special case $J = 0$ the function V is monotonically increasing in R between each of its infinitely many vertical asymptotes, and for every value of $V > 0$ there are infinitely many stable equilibrium profiles. However, only the solution on the first branch is physically realisable and so again there is only a single stable and physical equilibrium solution for all values of $V > 0$. Unlike the previous two cases the introduction of non-zero J changes this situation qualitatively.

Figure 11 shows J plotted against R for $V_0 = 20$, $V_0 = V_c \approx 32.4642$ and $V_0 = 40$. The branches in Fig. 11 can be classified as one of three types:

- J1 - a branch with a maximum/minimum "kink",
- J2 - a branch with a maximum turning point,
- J3 - a monotonically decreasing function.

The only order in which these branches can appear on each plot is J1 then J2 followed by J3 as R increases. Each branch lies between the vertical asymptotes of J, which occur at values of R satisfying

$$\begin{cases} \tan R = \dfrac{3R}{3 - R^2}, & (p) \\ \dfrac{J_1(R)}{J_0(R)} = \dfrac{4R}{8 - R^2}, & (a) \end{cases} \tag{35}$$

which are independent of V_0. The number of J1 branches depends on the value of V_0, whereas there is only ever one J2 branch and an infinite number of J3 branches extending to the right. The special value $V = V_c$ corresponds to the case where one of the vertical asymptotes of J disappears, leaving a continuous curve connecting what were two adjacent branches for $V < V_c$. Equating the numerator and denominator of Eq. (28) to zero we find that V_c satisfies

$$\begin{cases} \tan (3V_c)^{1/2} = \dfrac{3(3V_c)^{1/2}}{3 - 3V_c}, & (p) \\ \dfrac{J_1(2V_c^{1/3})}{J_0(2V_c^{1/3})} = \dfrac{8V_c^{1/3}}{8 - 4V_c^{2/3}}. & (a) \end{cases} \tag{36}$$

The values of R at which there is marginal stability are the solutions of Eq. (34) and, as the plots in Fig. 11 show, stable and physical solutions can occur on other branches as well as the first. Note that some of the regions of stability are relatively small. For example, in Fig. 11(a) there is a small stable but unphysical region between $R \approx 11.6198$ and $R \approx 11.9047$. As the drop profiles in Fig. 11 show, unlike in the zero-gravity and sessile cases, the solutions can become unphysical via $h = 0$ at locations other than the origin.

Figure 11(a) with $V_0 = 20$ shows one J2 branch and the first two of the J3 branches. In Fig. 11(b) V_0 is increased to V_c; the vertical asymptote at $R \approx 6.3802$ vanishes and a J2 branch and a J3 branch connect to form a critical J2 branch. In Fig. 11(c) V_0 is increased to 40 and the figure shows a J1, a J2 and the first J3 branch. Note that the number of J1 branches increases as V_0 increases, with the maximum/minimum kink occurring at smaller values of J as R increases. The drop profiles usually (but not always) have an increasing number of maxima and minima as R increases. For example, in Fig. 11(a) the drop profile on the J2 branch has one turning point and the drop profile on the J3 branch immediately to the right has five, whereas in Fig. 11(c) the drop profile on the J1 branch for $R \approx 6.3$ has five turning points while the drop profile on the J2 branch immediately to the right has only three. For any given value of J there are finitely many (at least one and possibly more) stable and physical profiles, and there is a maximum value of $J = J_m$ above which no physical and stable solutions exist.

Figure 12 shows V plotted against R for $J_0 = 0.12$, $J_0 = J_c \approx 0.1425$ and $J_0 = 0.16$, which can be described in a similar way to Fig. 11. The branches in Fig. 12 can be classified as one of three types:

- V1 - a monotonically increasing function,
- V2 - a branch with a maximum turning point,
- V3 - a branch with a minimum/maximum "kink".

The only order in which these branches can appear on each plot is V1 then V2 followed by V3 as R increases. Each branch lies between the vertical asymptotes of V, which occur at values of R satisfying

$$\begin{cases} \sin R = 0, & (p) \\ J_1(R) = 0, & (a) \end{cases} \tag{37}$$

which are independent of J_0. The number of V1 branches depends on the value of J_0, whereas there is only ever one V2 branch and an infinite number of V3 branches extending

to the right. The special value $J = J_c$ corresponds to the case where one of the vertical asymptotes of V disappears leaving a continuous curve connecting what were two adjacent branches for $J < J_c$. Equating the numerator and denominator of Eq. (27) to zero we find that J_c satisfies

$$\begin{cases} \sin\left(\dfrac{1}{J_c}\right) = 0, & (p) \\ J_1\left(\dfrac{1}{J_c}\right) = 0. & (a) \end{cases} \tag{38}$$

The values of R at which there is marginal stability are the solutions of Eq. (33) and, unlike in the case $J = 0$, stable and physical solutions can occur on branches other than just the first. Note that again some of the regions are relatively small. For example, in Fig. 12(a) there is a small unstable but physical region between $R \approx 4.9684$ and $R \approx 5.1356$. Once again the solutions can become unphysical via $h = 0$ at locations other than the origin.

Figure 12(a) with $J_0 = 0.12$ shows two V1 branches and a V2 branch with V3 branches extending infinitely to the right thereafter. In Fig. 12(b) J_0 is increased to J_c; the vertical asymptote $R = R_c \approx 7.0156$ vanishes, and a V1 branch and a V2 branch connect to form a critical V2 branch. In Fig. 12(c) J_0 is increased to 0.16 and the figure shows a V1, a V2 and the first V3 branch. Note that in this case the number of V1 branches decreases as J_0 increases while the minimum/maximum kink on the V3 branches occurs at ever larger values of V as R increases. As previously, the drop profiles usually (but not always) have an increasing number of maxima and minima as R increases. In this case for any given value of V there are finitely many (at least one and possibly more) stable and physical profiles, but there is no upper limit on the value of V for physical and stable solutions to exist.

Figure 13 plots contact angle θ against radius R in the case $V_0 = 20$ and $J_0 = 0.16$. The thick lines correspond to physical solutions and the thin lines correspond to unphysical solutions. The points of intersection with the horizontal line $\theta = 1$ correspond to equilibrium solutions at $R \approx 3.6524$ (stable), $R \approx 5.5740$ (stable) $R \approx 6.9149$ (unstable) and $R \approx 10.0041$ (unstable). Figure 14 plots examples of the evolution of the radius R as a function of time t obtained by solving Eq. (26) numerically in the particular case $F(\theta) = \theta^3 - 1$. The

shaded areas denote regions of unphysical solutions; our computations again exclude these regions. Figs. 15 and 16 show the evolution of the drop profile in the cases $R(0) = 1$ and $R(0) = 6.8$ respectively; in both figures the appropriate stable equilibrium solution is shown with a dashed curve.

Figure 17 plots contact angle θ against radius R for $V_0 = 20$ in the special case $J_0 = J_c \approx 0.1425$ and shows that, despite what the corresponding plot of V against R shown in Fig. 12(b) might suggest, the dynamics in this case are qualitatively similar to those when $J_0 = 0.12$ and $J_0 = 0.16$. Note, however, that when $J_0 = J_c$ there is, in general, no equilibrium solution with the correct volume with $R = R_c \approx 7.0156$, the value of R corresponding to the vertical asymptote of $V(R)$ that disappears when $J_0 = J_c$. Corresponding behaviour is observed when $V_0 = V_c$.

In all parts of Figs. 11 and 12 (but not the corresponding figures in the zero-gravity and sessile cases) there are evidently changes in stability at points other than the local extrema. Inspection of Eqs. (33) and (34) shows that these "unusual" changes of stability occur at points $R = R^*$ where $S(R^*) = 0$, and inspection of the definition of $S(R)$ in Eq. (23) shows that this is indeed possible only in the pendent case. Since $|\theta| \to \infty$ as these points are approached the lubrication approximation and possibly also (depending on the specific form of $F(\theta)$) the quasi-static approximation fail in the immediate vicinity of these points.

In the special case $J_0 = J_c$ (Fig. 12(b)) stability also changes at the point $R = R_c$ (the value of R corresponding to the vertical asymptote of $V(R)$ that disappears). Corresponding behaviour is again observed when $V_0 = V_c$.

VII. ANNULAR SOLUTIONS

A. Problem Formulation

As we have already seen, in many cases the solutions discussed thus far can fail to be physically-realisable via $h(0) = 0$. (Indeed, this is the only way that the solutions become

unphysical when $G^2 \geq 0$.) It is therefore natural to examine next the possibility of solutions that have a dry patch with no fluid near the origin. In an axisymmetic geometry these solutions take the form of an annular ring of fluid centered on $r = 0$, while in a planar geometry they take the form of two disconnected drops which are symmetric about $x = 0$. For convenience we shall use the term "annular" to describe both situations and the term "non-annular" to describe the solutions with $h(0) > 0$ discussed previously. In order to keep the algebra manageable we shall concentrate solely in this section on the special case of zero gravity, that is, the case $G = 0$. Clearly the major difference between the annular solutions discussed in this section and the non-annular solutions discussed previously is that the former have two contact lines and hence two contact angles. The outer contact line is located at $x = R_2(t)$ (p) or $r = R_2(t)$ (a) and the inner one at $x = R_1(t)$ (p) or $r = R_1(t)$ (a). The corresponding contact angles are denoted by $\theta = \theta(t)$ and $\phi = \phi(t)$. Physically-realisable solutions satisfy $\theta \geq 0$, $\phi \geq 0$ and $R_2 > R_1$, and in equilibrium $\theta = \theta_0$ and $\phi = \phi_0$. The geometry of the problem is summarised in Fig. 18.

Choosing the same scalings for the variables as before (see Sec. II) means that we can set $\theta_0 = 1$ without loss of generality. Furthermore, since we are considering only the case $G = 0$ we can, without loss of generality, set either $J = 1$ or $V = 1$; for ease of comparison with the earlier results and for clarity we shall retain both V and J in what follows and then present results for both $J = 1$ and $V = 1$. Hereafter scaled variables are used unless stated otherwise.

For quasi-static motion with $Q = 0$ at leading order in C the equation for h is given again by Eq. (18) with $G = 0$, namely

$$\begin{cases} h_{xxx} + Jx = 0, & (p) \\ \left(h_{rr} + \dfrac{h_r}{r}\right)_r + Jr = 0. & (a) \end{cases} \tag{39}$$

Since there are now two moving contact lines we need to replace Eq. (12) by two Tanner Laws relating the speed of each contact line to its contact angle. For these we use the forms

$$(R_1)_t = -F(\phi), \tag{40}$$

$$(R_2)_t = F(\theta), \tag{41}$$

where the empirically-determined function $F(\cdot)$ satisfies $F(1) = F(\phi_0) = 0$. Analogously to the non-annular case we assume that $F(\cdot)$ is monotonically-increasing locally near $\theta = 1$ and $\phi = \phi_0$, and so its first non-zero derivatives at both these points will be positive and of odd order. The boundary conditions for Eq. (39) are

$$h(R_1, t) = 0, \tag{42}$$

$$h(R_2, t) = 0, \tag{43}$$

$$\begin{cases} h_x(R_2, t) = -\theta, & (p) \\ h_r(R_2, t) = -\theta, & (a) \end{cases} \tag{44}$$

$$\begin{cases} h_x(R_1, t) = \phi, & (p) \\ h_r(R_1, t) = \phi. & (a) \end{cases} \tag{45}$$

Solving Eq. (39) subject to Eqs. (42) – (44) yields

$$h = \theta f(\cdot, R_1, R_2) + J g(\cdot, R_1, R_2), \tag{46}$$

where the symbol "$\cdot$" again denotes x (p) or r (a) and the functions $f(\cdot, R_1, R_2)$ and $g(\cdot, R_1, R_2)$ are given by

$$\begin{cases} f(x, R_1, R_2) = \dfrac{(R_2 - x)(R_1 - x)}{R_1 - R_2}, & (p) \\ f(r, R_1, R_2) = \dfrac{R_2(R_2^2 - r^2)\ln R_1 - R_2(R_1^2 - r^2)\ln R_2 - R_2(R_2^2 - R_1^2)\ln r}{R_2^2 - R_1^2 + 2R_2^2 \ln(R_1/R_2)}, & (a) \end{cases} \tag{47}$$

$$\begin{cases} g(x, R_1, R_2) = \dfrac{1}{24}(R_2 - x)^2(R_1 - x)(R_1 + 2R_2 + x), & (p) \\ g(r, R_1, R_2) = \dfrac{1}{32}\Big[-2R_2^2(R_2^2 - r^2)^2 \ln R_1 + 2R_2^2(R_2^2 - R_1^2)^2 \ln r \\ \qquad + 2R_2^2(R_1^2 - r^2)(2R_2^2 - R_1^2 - r^2)\ln R_2 \\ \qquad - (R_1^2 - r^2)(R_2^2 - r^2)(R_2^2 - R_1^2)\Big]\Big[R_2^2 - R_1^2 + 2R_2^2 \ln(R_1/R_2)\Big]^{-1}. & (a) \end{cases} \tag{48}$$

The volume of this annular drop is given by

$$\begin{cases} 2V = 2\displaystyle\int_{R_1}^{R_2} h\,\mathrm{d}x, & (p) \\ 2\pi V = 2\pi\displaystyle\int_{R_1}^{R_2} hr\,\mathrm{d}r, & (a) \end{cases} \tag{49}$$

and so

$$V = \theta S(R_1, R_2) + JT(R_1, R_2), \tag{50}$$

where the functions $S = S(R_1, R_2)$ and $T = T(R_1, R_2)$ are given by

$$S(R_1, R_2) = \begin{cases} \dfrac{(R_2 - R_1)^2}{6}, & (p) \\ \dfrac{R_2(R_2^4 - R_1^4)\ln(R_1/R_2) + R_2(R_2^2 - R_1^2)^2}{4[R_2^2 - R_1^2 + 2R_2^2\ln(R_1/R_2)]}, & (a) \end{cases} \tag{51}$$

$$T(R_1, R_2) = \begin{cases} -\dfrac{(2R_1 + 3R_2)(R_2 - R_1)^4}{360}, & (p) \\ -\dfrac{4R_2^2(2R_1^2 + R_2^2)(R_2^2 - R_1^2)^2\ln(R_1/R_2) + (R_1^2 + 5R_2^2)(R_2^2 - R_1^2)^3}{384[R_2^2 - R_1^2 + 2R_2^2\ln(R_1/R_2)]}. & (a) \end{cases} \tag{52}$$

We can trivially re-write Eq. (50) as an explicit expression for θ for constant $V = V_0$ and $J = J_0$ in the form

$$\theta = \frac{V_0 - J_0 T(R_1, R_2)}{S(R_1, R_2)}. \tag{53}$$

The remaining boundary condition Eq. (45) yields an explicit expression for ϕ for constant $V = V_0$ and $J = J_0$ in the form

$$\phi = \begin{cases} \theta - \dfrac{J_0}{12}(R_2 + R_1)(R_2 - R_1)^2, & (p) \\ \Big[(R_2^2 - R_1^2)\left[R_2^4 - R_1^4 + 4R_1^2R_2^2\ln(R_1/R_2)\right]J_0 & \\ -16R_2\left[R_2^2 - R_1^2 + 2R_1^2\ln(R_1/R_2)\right]\theta\Big]\Big[16R_1[R_2^2 - R_1^2 + 2R_2^2\ln(R_1/R_2)]\Big]^{-1}. & (a) \end{cases} \tag{54}$$

Evidently in equilibrium ($\theta = 1$, $\phi = \phi_0$) annular solutions are impossible in the planar case if $\phi_0 \geq 1$; in particular, there is no non-trivial annular solution in the case in which the contact angles are equal, that is, when $\phi_0 = 1$. Indeed, from Eq. (54)(p) it is clear that equilibrium annular solutions with equal inner and outer contact angles are possible only when $J_0 = 0$. The explanation for this is that in the planar case the "annulus" comprises two

disconnected drops, symmetrically placed about $x = 0$, each of them subject to an off-center jet; such a drop cannot be in equilibrium when $\theta_0 = \phi_0$ since the net external force on it is nonzero (because the resultant force due to the jet has a nonzero x-component, whereas the x-components of the surface-tension forces at the two contact lines cancel each other out exactly when $\theta_0 = \phi_0$). As we shall see there is no similar restriction on the value of ϕ_0 for annular solutions in the axisymmetric case.

In the planar case Eqs. (53) and (54) yield

$$\theta = \frac{360V_0 + (3R_2 + 2R_1)(R_2 - R_1)^4 J_0}{60(R_2 - R_1)^2}, \tag{55}$$

$$\phi = \frac{360V_0 - (2R_2 + 3R_1)(R_2 - R_1)^4 J_0}{60(R_2 - R_1)^2}, \tag{56}$$

while in the axisymmetric case they yield

$$\theta = \frac{\tau_1(R_1, R_2)J_0 + \tau_2(R_1, R_2)V_0}{96R_2(R_2^2 - R_1^2)[R_2^2 - R_1^2 + (R_1^2 + R_2^2)\ln(R_1/R_2)]}, \tag{57}$$

$$\phi = \frac{\tau_3(R_1, R_2)J_0 + \tau_4(R_1, R_2)V_0}{96R_1(R_2^2 - R_1^2)[R_2^2 - R_1^2 + (R_1^2 + R_2^2)\ln(R_1/R_2)]}, \tag{58}$$

where the functions τ_1, τ_2, τ_3 and τ_4 are given by

$$\left.\begin{aligned}
\tau_1(R_1, R_2) &= (R_2^2 - R_1^2)^2[5R_2^4 - 4R_1^2R_2^2 - R_1^4 + (4R_2^4 + 8R_1^2R_2^2)\ln(R_1/R_2)], \\
\tau_2(R_1, R_2) &= 384[R_2^2 - R_1^2 + 2R_2^2\ln(R_1/R_2)], \\
\tau_3(R_1, R_2) &= (R_2^2 - R_1^2)^2[R_2^4 + 4R_1^2R_2^2 - 5R_1^4 + (4R_1^4 + 8R_2^2R_1^2)\ln(R_1/R_2)], \\
\tau_4(R_1, R_2) &= -384[R_2^2 - R_1^2 + 2R_1^2\ln(R_1/R_2)].
\end{aligned}\right\} \tag{59}$$

Note that in the limit $R_1, R_2 \to \infty$ for fixed $R_2 - R_1 > 0$ we recover the previous results for the planar case, while in the limit $R_2 \to \infty$ for fixed R_1 we obtain the special case of a hole in an unbounded fluid film corresponding to the thin-film limit of the zero-gravity version of the problem studied by Taylor and Michael[36] and Wilson and Duffy[37].

B. Stability Analysis

Proceeding as in the non-annular case we can determine the stability of an equilibrium drop for which $\theta = 1$, $\phi = \phi_0$, $R_1 = R_1^0$ and $R_2 = R_2^0$ to small perturbations in R_1 and R_2

by writing $R_1(t) = R_1^0 + R_1^1(t)$ and $R_2(t) = R_2^0 + R_2^1(t)$ and expanding Eqs. (40) and (41) for small R_1^1 and R_2^1 to yield

$$\begin{cases} (R_1^1)_t = -\dfrac{M}{m!}(\alpha_1 R_1^1 + \alpha_2 R_2^1)^m, \\ (R_2^1)_t = \dfrac{N}{n!}(\beta_1 R_1^1 + \beta_2 R_2^1)^n, \end{cases} \tag{60}$$

where $M = \mathrm{d}^m F(\phi)/\mathrm{d}\phi^m|_{\phi=\phi_0} > 0$ $(m = 1, 3, 5, \ldots)$ is the first non-zero derivative of $F(\phi)$ evaluated at $\phi = \phi_0$, and $N = \mathrm{d}^n F(\theta)/\mathrm{d}\theta^n|_{\theta=1} > 0$ $(n = 1, 3, 5, \ldots)$ is the first non-zero derivative of $F(\theta)$ evaluated at $\theta = 1$, and the constants α_1, α_2, β_1 and β_2 are given by $\alpha_i = \partial\phi/\partial R_i$ and $\beta_i = \partial\theta/\partial R_i$ evaluated at $R_1 = R_1^0$ and $R_2 = R_2^0$ for $i = 1, 2$. As before, we shall immediately drop the clumsy superscript notation and in the remainder of this section we shall denote R_1^0 and R_2^0 simply by R_1 and R_2. Unfortunately, unlike in the non-annular case, we have been unable to obtain either the general solution of Eq. (60) or general criteria for the growth or decay of the solutions of Eq. (60) as $t \to \infty$. However, we can make progress in the special case $m = n = 1$ when the system given by Eq. (60) is linear and has eigenvalues

$$\lambda_\pm = \frac{N\beta_2 - M\alpha_1 \pm \left[(M\alpha_1 + N\beta_2)^2 - 4MN\alpha_2\beta_1\right]^{\frac{1}{2}}}{2}, \tag{61}$$

and so stability of the equilibrium solution is determined by the sign of $\mathrm{Re}(\lambda_+)$. Hereafter we shall take $M = N = 1$ for simplicity.

1. Planar case

In the planar case we can use Eqs. (55) and (56) to evaluate the α_i and β_i for $i = 1, 2$ and hence obtain simple explicit expressions for $\lambda_\pm$, namely

$$\lambda_+ = \frac{J_0}{12}(R_2 - R_1)^2, \tag{62}$$

$$\lambda_- = \frac{J_0}{20}(R_2 - R_1)^2 - \frac{24V_0}{(R_2 - R_1)^3}. \tag{63}$$

Note that λ_+ is independent of V_0 in this case. We can deduce immediately that the eigenvalues $\lambda_\pm$ are purely real and, since $\lambda_+ > 0$ for all values of V_0 and J_0, that all planar annular solutions are unconditionally unstable.

2. Axisymmetric case

In the axisymmetric case we can use Eqs. (57), (58) and (59) to evaluate the α_i and β_i for $i = 1, 2$ and hence obtain the corresponding expressions for $\lambda_\pm$. However, these expressions are now very lengthy and considerably more effort is required to establish the sign of $\mathrm{Re}(\lambda_+)$ than in the planar case. Details are given in the Appendix, where it is shown that $\lambda_\pm$ are purely real and that $\lambda_+ > 0$ for all R_1 and R_2. Hence all axisymmetric annular solutions are unconditionally unstable, just as in the planar case.

C. Results

1. Explanation of Figures

In Figs. 19–22 we present plots of jet strength J against outer radius R_2 for fixed volume $V_0 = 1$, and volume V against outer radius R_2 for fixed jet strength $J_0 = 1$. Note that all the annular solutions depicted in Figs. 19–22 are physically realisable and unstable, and therefore represented by thick dashed lines. Each of these plots contain annular solutions for various inner contact angles ϕ_0. Since $\theta_0 = 1$, values of ϕ_0 other than $\phi_0 = 1$ require that either the system exhibits contact-angle hysteresis (with $\theta_r \leq \theta_0 \leq \theta_a$, where θ_r and θ_a are the receding and advancing contact angles respectively) or, more artificially, that the substrate be inhomogeneous with a change of physical properties somewhere in $R_1 < r < R_2$. The case $\phi_0 = 1$, however, requires no such conditions. In each plot, curve (A) corresponds to the physically-realisable non-annular solutions as discussed in Sec. VI B. In the planar case (Figs. 19 and 20) curve (B) corresponds to solutions with $R_1 = 0$, representing two contiguous drops, one in $-R_2 \leq x \leq 0$ and the other in $0 \leq x \leq R_2$. In the axisymmetric case, however, the only solution with $R_1 = 0$ occurs when $\phi_0 = 0$, and so there is no curve in Figs. 21 and 22 corresponding to curve (B) in Figs. 19 and 20. Figure 23 shows examples of the evolution of the radii R_1 and R_2 as functions of time in the axisymmetric case for a particular choice of $F(\theta)$, while Figs. 24 and 25 show corresponding examples of the

evolution of the profile of the annular drop. Unlike for the non-annular solutions described in Sec. VI, the qualitative behaviour of the planar and axisymmetric annular solutions are quite different, and so in what follows we discuss these two cases separately.

2. Planar Case

Figure 19 shows a plot of J against R_2 when $V_0 = 1$ for inner contact angles $\phi_0 = 0.2$, 0.7, 0.9 and 0.99. In particular, Fig. 19 shows how each annular curve branches away from curve (B) at a different point. Note that, as previously indicated, there are no non-trivial annular solutions for $\phi_0 \geq 1$, and that as $\phi_0 \to 1^-$ the corresponding J against R_2 curve approaches the $J = 0$ axis. For all the annular curves $J \sim (1 - \phi_0^2)/2R_2$ as $R_2 \to \infty$.

Figure 20 shows a plot of V against R_2 when $J_0 = 1$ for inner contact angles $\phi_0 = 0.2$, 0.7, 0.9 and 0.99, and again shows how each annular curve branches away from curve (B) at a different point. As $\phi_0 \to 1^-$ the corresponding V against R_2 curve approaches the $V = 0$ axis. For all the annular curves $V \sim (1 - \phi_0^2)/2R_2$ as $R_2 \to \infty$.

3. Axisymmetric Case

Figure 21 shows a plot of J against R_2 when $V_0 = 1$ for inner contact angles $\phi_0 = 0.5$, 0.8, 1, 1.1 and 1.3, and shows how all the annular curves branch away from the non-annular curve (A) at the single point $R_2 = 24^{1/3}$ and $J = 2/3$ where the non-annular solutions fail to be physical via $h(0) = 0$. Unlike in the planar case, annular solutions are now possible for all values of $\phi_0 \geq 0$. Whatever the value of ϕ_0 we have $J \sim (1 - \phi_0^2)/2$ as $R_2 \to \infty$, and so only those curves for $0 \leq \phi_0 \leq 1$ approach a non-negative limiting value J as $R_2 \to \infty$; curves for $\phi_0 > 1$ cross the $J = 0$ axis at a finite value of $R_2 > 0$.

Figure 22 shows a plot of V against R_2 when $J_0 = 1$ for inner contact angles $\phi_0 = 0.7$, 0.9, 1, 1.02, 1.3 and 1.5, and again shows how all the annular curves branch away from the non-annular curve (A) at the single point $R_2 = 16^{1/3}$ and $V = 2/3$ where the non-annular solutions fail to be physical via $h(0) = 0$. Figure 22 also shows that the curves corresponding

to $0 \leq \phi_0 \leq 1$ and $\phi_0 > 1$ have qualitatively different behaviour. When $0 \leq \phi_0 \leq 1$ we have $V \sim (1 - \phi_0^2)/2$ as $R_2 \to \infty$, and hence these curves approach a non-negative limiting value as $R_2 \to \infty$. On the other hand, when $\phi_0 > 1$ we have

$$V \sim \frac{(1 - A^2)^2 + (1 - A^4) \ln A}{4(1 - A^2 + 2 \ln A)} R_2^3 \tag{64}$$

as $R_2 \to 0$, where the unique value of A depends on the value of ϕ_0 via the equation

$$\frac{1 - A^2 + 2A^2 \ln A}{A(1 - A^2 + 2 \ln A)} + \phi_0 = 0. \tag{65}$$

Figure 23 plots examples of the evolution of the inner radius R_1 and the outer radius R_2 as functions of time t obtained by numerically solving Eqs. (40) and (41) in the particular case $F(\theta) = \theta^3 - 1$ and $F(\phi) = \phi^3 - 1$ (i.e. equal equilibrium contact angles) for $J_0 = 1$ and $V_0 = 0.1696$. The horizontal dashed lines correspond to the equilibrium values $R_1 \approx 1.1968$, $R_2 = 2$. The thick lines correspond to the curves with initial conditions $R_1(0) = 1$, $R_2(0) = 1.7$, the thin lines correspond to $R_1(0) = 1$, $R_2(0) = 2.2$, the dashed lines correspond to $R_1(0) = 1.3$, $R_2(0) = 1.7$ and the dot-dashed lines correspond to $R_1(0) = 1.3$, $R_2(0) = 2.2$. These examples illustrate what we found in all the cases that we investigated (with different initial conditions), namely that annular drops 'close' if the initial outer radius $R_2(0)$ is smaller than the equilibrium value and 'open' if $R_2(0)$ is larger than the equilibrium value, irrespective of the value of the initial inner radius $R_1(0)$. This behaviour was also found in cases with different values of the inner equilibrium contact angle ϕ_0. Figures 24 and 25 show the evolution of the annular drop profile in the cases $R_1(0) = 1.3$, $R_2(0) = 1.7$ and $R_1(0) = 1.3$, $R_2(0) = 2.2$ respectively, and show how the annular drop with initial outer radius smaller than the equilibrium value 'closes' and the annular drop with initial outer radius larger than the equilibrium value 'opens'.

VIII. CONCLUSIONS

In this paper we investigated the quasi-static spreading of a finite-sized thin drop of incompressible, Newtonian fluid attached to a planar substrate in the presence of a jet of air

in both symmetric two-dimensional and axisymmetric three-dimensional geometries. Three specific problems were studied in detail: a jet of air acting normally to the substrate when gravity effects are negligible, a jet of air directed vertically downwards onto a sessile drop on a horizontal substrate and a jet of air directed vertically upwards onto a pendent drop on a horizontal substrate. For the simple model of the jet we adopted, the axisymmetric air-jet-blowing problem is identical to the axisymmetric spin-coating problem, and so the results in the axisymmetric case also apply to the spin-coating problem. For each problem we investigated the possible physically-realisable non-annular equilibrium solutions for the profile of the drop and investigated their stability to small perturbations. We also investigated the existence and stability of annular solutions in the zero-gravity case.

We found that for non-annular drops, the zero-gravity and sessile drop cases are qualitatively similar, and in both cases there is at most one stable and physical equilibrium solution in the presence of the air jet. An equilibrium solution for a drop with fixed volume V is possible only if the jet strength J is sufficiently small and an equilibrium solution for a drop with fixed J is possible only if V is sufficiently small. In the case of a non-annular pendent drop there are finitely many (at least one and possibly more) stable and physical equilibrium solutions. Stable and physical equilibrium solutions for a drop with fixed V are possible only if J is sufficiently small, but stable and physical equilibrium solutions for a drop with fixed J are possible for all values of V.

Unlike the non-annular drops, it was found that the planar and axisymmetric annular drops in zero gravity exhibit qualitatively different characteristics. In the planar case, it was shown that there are no equilibrium solutions when the inner contact angle is equal to or greater than the outer one, while in the axisymmetric case equilibrium solutions are possible for all values of the inner contact angle. As in the zero-gravity non-annular case, equilibrium annular solutions for fixed V are possible only for sufficiently small J, and for fixed J are possible only for sufficiently small V. However, in all the cases we investigated we showed that in both planar and axisymmetric geometries, all these annular solutions are unconditionally unstable. Quasi-static evolutions of these annular drops were calculated

numerically, and it was found in all the cases investigated that drops with initial outer radius smaller than that of the equilibrium value closed while drops with initial outer radius larger than the equilibrium value opened, irrespective of the value of the initial inner radius. The analysis of annular solutions was restricted to the special case of zero gravity.

The present work can clearly be extended in a number of interesting ways. Firstly, the stability analysis presented here was restricted to the quasi-static limit of small capillary number $C \to 0$. The obvious next step is to undertake a more general stability analysis for non-zero values of C. Typically, this approach gives rise to a high-order differential equation of the type investigated by, for example, Hocking and Miksis[38] and López *et al.*[25–27], which must, in general, be solved numerically. Secondly, the stability of solutions to non-axisymmetric perturbations (thus including the fingering instabilities described in Sec. I) should also be examined. Thirdly, the model for the air jet could be improved in order to make it more realistic. For simplicity, we assumed zero shear stress at the drop surface; a more accurate model would include a non-zero shear due to the jet of air. Fourthly, the analysis of the annular solutions, undertaken here only in the special case $G = 0$, should be extended to $G \neq 0$ in order to investigate both sessile and pendent situations.

ACKNOWLEDGMENTS

During the course of the present work the first author (ISM) was supported by the University of Strathclyde, Glasgow, Scotland, UK, via the Graduate Teaching Assistant Scheme. This work was completed while the second author (SKW) was a Visiting Scholar in the Department of Engineering Science and Applied Mathematics of Northwestern University, Evanston, IL, USA, where he was partially supported under a United States Department of Energy Grant in the Basic Energy Sciences while he was visiting Prof. S. G. Bankoff and Prof. S. H. Davis.

APPENDIX: STABILITY ANALYSIS FOR AN AXISYMMETRIC ANNULAR DROP

In this appendix we analyse the linear stability of an axisymmetric annular drop in the case $m = n = 1$. Specifically we show that the eigenvalues $\lambda_\pm$ (defined in Eq. (61) with $M = N = 1$) are purely real and that $\lambda_+ > 0$. To simplify the subsequent algebra we write $R_1 = \eta$, $R_2 = c\eta$ and so the requirements that $R_1 > 0$, $R_2 > 0$ and $R_2 > R_1$ mean that $\eta > 0$ and $c > 1$.

Firstly, we demonstrate that $\lambda_\pm$ are purely real. If we denote the discriminant of $\lambda_\pm$ by $D_1 = (\alpha_1 + \beta_2)^2 - 4\alpha_2\beta_1$ then by setting $J_0 = 1$ without loss of generality we can write

$$D_1 = \frac{1}{\eta^8}\left[\nu_1(c)V_0^2 + \eta^6\nu_2(c)V_0 + \eta^{12}\nu_3(c)\right], \tag{A1}$$

where ν_1, ν_2 and ν_3 are known functions of c, not reproduced here for brevity. Evidently D_1 can change sign only when V_0 satisfies

$$\nu_1(c)V_0^2 + \eta^6\nu_2(c)V_0 + \eta^{12}\nu_3(c) = 0. \tag{A2}$$

Thus the existence or non-existence of real solutions for V_0 depends on the sign of the discriminant D_2 of Eq. (A2), which is given by

$$\begin{aligned} D_2 = \eta^{12}(c^4 - 4c^2\ln c - 1)^2\Big[&(7c^2-1)(c^2-7)(c^2-1)^3 \\ &- 3(c^2+1)(c^4-22c^2+1)(c^2-1)^2\ln c - 8c^2(c^2-1)(5c^4-4c^2+5)(\ln c)^2 \\ &- 48c^4(c^2+1)(\ln c)^3\Big]\Big[c^4(c^2-1)^2(c^2\ln c - c^2 + \ln c + 1)^5\Big]^{-1}. \end{aligned} \tag{A3}$$

Note that $D_2 \sim O(-(c-1)^{-2})$ as $c \to 1^+$ and $D_2 \sim O(-(\ln c)^{-4})$ as $c \to \infty$. Evidently the sign of D_2 depends only on c and not on η. Figure 26 shows a plot of D_2 as a function of $c > 1$ and clearly demonstrates that $D_2 < 0$ for all values of c. Hence there are no real roots of Eq. (A2) and therefore D_1 is of one sign. A simple evaluation of D_1 with values $V_0 > 0$ and $c > 1$ shows that it is always positive and hence the eigenvalues $\lambda_\pm$ are always real.

Secondly, we demonstrate that $\lambda_+ > 0$. From Eq. (61) we can write

$$\lambda_{\pm} = \gamma_1(c)\eta^2 + \frac{\gamma_2(c)}{\eta} \pm \left[\gamma_3(c)\eta^4 + \gamma_4(c)\eta + \frac{\gamma_5(c)}{\eta^2}\right]^{\frac{1}{2}}, \tag{A4}$$

where the γ_i, $i = 1 \ldots 5$ are known functions of c, not reproduced here for brevity. Typical values of $\lambda_{\pm}$ are plotted as functions of η for a range of values of c in Fig. 27. Of most importance are the minimum value of λ_+ (denoted by $\lambda_{\min}$) and the maximum value of λ_- (denoted by $\lambda_{\max}$) and numerically calculated values of these quantities are shown in Fig. 28. Note that $\lambda_{\min} \sim 2^{-1/3}$ and $\lambda_{\max} \sim 2^{-1/3}$ as $c \to \infty$ while $\lambda_{\min} \sim O((c-1)^{5/3})$ and $\lambda_{\max} \sim O(-(c-1)^{5/3})$ as $c \to 1^+$. As Fig. 28 shows, $\lambda_{\max} < 0$ when $1 < c < c_{\text{crit}}$ and $\lambda_{\max} > 0$ when $c > c_{\text{crit}}$, where $c = c_{\text{crit}} \simeq 31.05$ is the single real root of the equation

$$(c^2 - 4c + 1)\ln c - 3c^2 + 3 = 0. \tag{A5}$$

More significantly, Fig. 28 also shows that $\lambda_{\min} > 0$ for all $c > 1$ and so $\lambda_+ \geq \lambda_{\min} > 0$ for $c > 1$; therefore all axisymmetric annular solutions are unconditionally unstable, just as in the planar case.

REFERENCES

[1] A. G. Emslie, F. T. Bonner, and L. G. Peck, "Flow of a viscous liquid on a rotating disk," J. Appl. Phys. **29**, 858 (1958).

[2] M. Yanagisawa, "Slip effect for thin liquid film on a rotating disk," J. Appl. Phys. **61**, 1034 (1987).

[3] Y.-O. Tu, "Contact line slippage of fluid flow on a rotating disk," J. Coll. Int. Sci. **116**, 237 (1987).

[4] A. Acrivos, M. J. Shah, and E. E. Petersen, "On the flow of a non-Newtonian liquid on a rotating disk," J. Appl. Phys. **31**, 963 (1960).

[5] C. J. Lawrence, "The mechanics of spin coating of polymer films," Phys. Fluids **31**, 2786 (1988).

[6] C. J. Lawrence and W. Zhou, "Spin coating of non-Newtonian fluids," J. Non-Newtonian Fluid Mech. **39**, 137 (1991).

[7] S. A. Jenekhe and S. B. Schuldt, "Flow and film thickness of Bingham plastic liquids on a rotating disk," Chem. Eng. Commun. **33**, 135 (1985).

[8] S. L. Burgess and S. D. R. Wilson, "Spin coating of a viscoplastic material," Phys. Fluids **8**, 2291 (1996).

[9] D. Meyerhofer, "Characteristics of resist films produced by spinning," J. Appl. Phys. **49**, 3993 (1978).

[10] B. G. Higgins, "Film flow on a rotating disk," Phys. Fluids **29**, 3522 (1986).

[11] D. E. Bornside, C. W. Macosko, and L. E. Scriven, "Spin coating : One-dimensional model," J. Appl. Phys. **66**, 5185 (1989).

[12] B. Reisfeld, S. G. Bankoff, and S. H. Davis, "The dynamics and stability of thin liquid

films during spin coating 1. Films with constant rates of evaporation or absorption," J. Appl. Phys. **70**, 5258 (1991).

[13] S. M. Troian, E. Herbolzheimer, S. A. Safran, and J. F. Joanny, "Fingering instabilities of driven spreading films," Europhys. Lett. **10**, 25 (1989).

[14] J. A. Moriarty, L. W. Schwartz, and E. O. Tuck, "Unsteady spreading of thin liquid films with small surface tension," Phys. Fluids A **3**, 733 (1991).

[15] N. Fraysse and G. M. Homsy, "An experimental study of rivulet instabilities in centrifugal spin coating of viscous Newtonian and non-Newtonian fluids," Phys. Fluids **6**, 1491 (1994).

[16] C. H. Ellen and C. V. Tu, "An analysis of jet stripping of liquid coatings," J. Fluids Eng. **106**, 339 (1984).

[17] E. O. Tuck and J.-M. Vanden Broeck, "Influence of surface tension on jet stripped continuous coating of sheet materials," A. I. Ch. E. Journal **30**, 808 (1984).

[18] J-M. Buchlin, M. Manna, M. Arnalsteen, M. L. Reithmuller, and M. Dubois, "Theoretical and experimental investigation of gas-jet wiping," in *First European Coating Symposium on The Mechanics of Thin Film Coatings, Leeds University, UK, 19-22 September 1995*, edited by P. H. Gaskell, M. D. Savage, J. L. Summers, (World Scientific, Singapore, 1996), pp. 168-178.

[19] L. M. Hocking, "Rival contact-angle models and the spreading of drops," J. Fluid Mech. **239**, 671 (1992).

[20] H. P. Greenspan, "On the motion of a small viscous droplet that wets a surface," J. Fluid Mech. **84**, 125 (1978).

[21] P. Ehrhard and S. H. Davis, "Non-isothermal spreading of liquid drops on horizontal plates," J. Fluid Mech. **229**, 365 (1991).

[22] P. Ehrhard, "The spreading of hanging drops," J. Colloid Interface Sci. **168**, 242 (1994).

[23] R. J. Braun, B. T. Murray, W. J. Boettinger, and G. B. McFadden, "Lubrication theory for reactive spreading of a thin drop," Phys. Fluids **7**, 1797 (1995).

[24] S. K. Wilson and E. L. Terrill, "The dynamics of planar and axisymmetric holes in thin fluid layers," in *First European Coating Symposium on The Mechanics of Thin Film Coatings, Leeds University, UK, 19-22 September 1995*, edited by P. H. Gaskell, M. D. Savage, J. L. Summers, (World Scientific, Singapore, 1996), pp. 288-297.

[25] P. G. López, M. J. Miksis, and S. G. Bankoff, "Stability and evolution of a dry spot," Northwestern University Applied Mathematics Technical Report 9605 (July 1997).

[26] P. G. López, S. G. Bankoff, and M. J. Miksis, "Non-isothermal spreading of a thin liquid film on an inclined plane," J. Fluid Mech. **324**, 261 (1996).

[27] P. G. López., M. J. Miksis, and S. G. Bankoff, "Inertial effects on contact line instability in the coating of a dry inclined plane," Phys. Fluids **9**, 2177 (1997).

[28] S. K. Wilson and B. R. Duffy, "On the gravity-driven draining of a rivulet of viscous fluid down a slowly varying substrate with variation transverse to the direction of flow," Phys. Fluids **10**, 13 (1998).

[29] L. M. Hocking, "Sliding and spreading of thin two-dimensional drops," Q. Jl Mech. appl. Math. **34**, 37 (1981).

[30] L. M. Hocking, "The spreading of a thin drop by gravity and capillarity," Q. Jl Mech. appl. Math. **36**, 55 (1983).

[31] L. M. Hocking, "The spreading of drops with intermolecular forces," Phys. Fluids **6**, 3224 (1994).

[32] Y. D. Shikhmurzaev, "Moving contact lines in liquid/liquid/solid systems," J. Fluid Mech. **334**, 211 (1997).

[33] Y. D. Shikhmurzaev, "Spreading of drops on solid surfaces in a quasi-static regime, "

Phys. Fluids **9**, 266 (1997).

[34] A. Oron, S. H. Davis and S. G. Bankoff, "Long-scale evolution of thin liquid films," Rev. Mod. Phys. **69**, 931 (1997).

[35] B. R. Duffy and S. K. Wilson, "A third-order differential equation arising in thin-film flows and relevant to Tanner's Law," Appl. Math. Lett. **10**, 3 (1997).

[36] G. I. Taylor and D. H. Michael, "On making holes in a sheet of fluid," J. Fluid Mech. **58**, 625 (1973).

[37] S. K. Wilson and B. R. Duffy, "An asymptotic analysis of small holes in thin fluid layers," J. Eng. Math. **30**, 445 (1996).

[38] L. M. Hocking, and M. J. Miksis, "Stability of a ridge of fluid," J. Fluid Mech. **247**, 157 (1993).

FIGURES

FIG. 1. Geometry of the non-annular problem.

FIG. 2. Plot of jet strength J against radius R for an axisymmetric drop in the case of zero gravity for $V_0 = 1, 2, 3$. The line styles are defined in Sec. VI A. Typical drop profiles are given in Fig. 3.

FIG. 3. Typical drop profiles for various values of radius R for a drop in zero gravity. Drop profiles in the sessile drop case are qualitatively similar to those shown here.

FIG. 4. Plot of volume V against radius R for an axisymmetric drop in the case of zero gravity for $J_0 = 1, 2, 3$. The line styles are defined in Sec. VI A. Typical drop profiles are given in Fig. 3.

FIG. 5. Plot of contact angle θ against radius R for an axisymmetric drop in the case of zero gravity, with $V_0 = 0.4$ and $J_0 = 1$. The thick line corresponds to physical solutions; the thin line corresponds to unphysical solutions. The points of intersection with the horizontal line $\theta = 1$ correspond to equilibrium solutions.

FIG. 6. Examples of the evolution of drop radius $R(t)$ for an axisymmetric drop in the case of zero gravity when $V_0 = 0.4$ and $J_0 = 1$ obtained by solving Eq. (26) numerically in the case $F(\theta) = \theta^3 - 1$. The equilibrium values $R \approx 1.5608$ (stable) and $R \approx 2.7233$ (unstable) are indicated by horizontal dashed lines, and the shaded area denotes a region of unphysical solutions.

FIG. 7. Evolution of a quasi-static drop profile for an axisymmetric drop in the case of zero gravity when $V_0 = 0.4$, $J_0 = 1$, with the initial condition $R(0) = 0.5$. The dashed curve corresponds to the stable equilibrium solution $R \approx 1.5608$.

FIG. 8. Evolution of a quasi-static drop profile for an axisymmetric drop in the case of zero gravity when $V_0 = 0.4$, $J_0 = 1$, with the initial condition $R(0) = 2.3$. The dashed curve corresponds to the stable equilibrium solution $R \approx 1.5608$.

FIG. 9. Plot of jet strength J against radius R for an axisymmetric sessile drop for $V_0 = 1, 2, 3$. The line styles are defined in Sec. VI A. Drop profiles in this case are qualitatively similar to those shown in Fig. 3.

FIG. 10. Plot of volume V against radius R for an axisymmetric sessile drop for $J_0 = 1, 2, 3$. The line styles are defined in Sec. VI A. Drop profiles in this case are qualitatively similar to those shown in Fig. 3.

FIG. 11. Plot of jet strength J against radius R for an axisymmetric pendent drop when (a) $V_0 = 20 < V_c$, (b) $V_0 = V_c \approx 32.4642$ and (c) $V_0 = 40 > V_c$. The line styles are defined in Sec. VI A.

FIG. 12. Plot of volume V against radius R for an axisymmetric pendent drop when (a) $J_0 = 0.12 < J_c$, (b) $J_0 = J_c \approx 0.1425$ and (c) $J_0 = 0.16 > J_c$. The line styles are defined in Sec. VI A.

FIG. 13. Plot of contact angle θ against radius R for an axisymmetric pendent drop, with $V_0 = 20$ and $J_0 = 0.16$. The thick lines correspond to physical solutions; the thin lines correspond to unphysical solutions. The points of intersection with the horizontal line $\theta = 1$ correspond to equilibrium solutions.

FIG. 14. Examples of the evolution of drop radius $R(t)$ for an axisymmetric pendent drop when $V_0 = 20$ and $J_0 = 0.16$, obtained by solving Eq. (26) numerically in the case $F(\theta) = \theta^3 - 1$. The equilibrium values $R \approx 3.6524$ (stable), $R \approx 5.5740$ (stable), $R \approx 6.9149$ (unstable) and $R \approx 10.0041$ (unstable) are indicated by horizontal dashed lines, and the shaded areas denote regions of unphysical solutions.

FIG. 15. Evolution of a quasi-static drop profile for an axisymmetric pendent drop when $V_0 = 20$, $J_0 = 0.16$, with the initial condition $R(0) = 1$. The dashed curve corresponds to the stable equilibrium solution $R \approx 3.6524$.

FIG. 16. Evolution of a quasi-static drop profile for an axisymmetric pendent drop when $V_0 = 20$, $J_0 = 0.16$, with the initial condition $R(0) = 6.8$. The dashed curve corresponds to the stable equilibrium solution $R \approx 5.5740$.

FIG. 17. Plot of contact angle θ against radius R for an axisymmetric pendent drop, with $V_0 = 20$ and $J_0 = J_c \approx 0.1425$. The thick lines correspond to physical solutions; the thin lines correspond to unphysical solutions. The points of intersection with the horizontal line $\theta = 1$ correspond to equilibrium solutions. The open circle ($\circ$) indicates that there is no solution with the correct volume at this special value of $R = R_c \approx 7.0156$.

FIG. 18. Geometry of the annular problem.

FIG. 19. Plot of jet strength J against outer radius R_2 for a planar annular drop for $\phi_0 = 0.2$, 0.7, 0.9 and 0.99 when $V_0 = 1$ and $G = 0$. A solid, thick line represents stable and physical equilibrium solutions; a dashed, thick line represents unstable and physical solutions. Curve (A) corresponds to physically-realisable non-annular solutions and curve (B) corresponds to solutions for two physically-realisable contiguous drops.

FIG. 20. Plot of volume V against outer radius R_2 for a planar annular drop for $\phi_0 = 0.2$, 0.7, 0.9 and 0.99 when $J_0 = 1$ and $G = 0$. A solid, thick line represents stable and physical equilibrium solutions; a dashed, thick line represents unstable and physical solutions. Curve (A) corresponds to physically-realisable non-annular solutions and curve (B) corresponds to solutions for two physically-realisable contiguous drops.

FIG. 21. Plot of jet strength J against outer radius R_2 for an axisymmetric annular drop for $\phi_0 = 0.5$, 0.8, 1, 1.1 and 1.3 when $V_0 = 1$ and $G = 0$. A solid, thick line represents stable and physical equilibrium solutions; a dashed, thick line represents unstable and physical solutions. Curve (A) corresponds to physically-realisable non-annular solutions.

FIG. 22. Plot of volume V against outer radius R_2 for an axisymmetric annular drop for $\phi_0 = 0.7$, 0.9, 1, 1.02, 1.1 and 1.3 when $J_0 = 1$ and $G = 0$. A solid, thick line represents stable and physical equilibrium solutions; a dashed, thick line represents unstable and physical solutions. Curve (A) corresponds to physically-realisable non-annular solutions.

FIG. 23. Examples of the evolution of drop radii $R_1(t)$ and $R_2(t)$ for an axisymmetric annular drop in the case of zero gravity when $J_0 = 1$ and $V_0 = 0.1696$, obtained by solving Eqs. (40) and (41) numerically in the case $F(\theta) = \theta^3 - 1$ and $F(\phi) = \phi^3 - 1$. The unstable equilibrium values $R_1 \approx 1.1968$, $R_2 = 2$ are indicated by horizontal dashed lines. The initial conditions are $R_1(0) = 1$, $R_2(0) = 1.7$ (thick lines), $R_1(0) = 1$, $R_2(0) = 2.2$ (thin lines), $R_1(0) = 1.3$, $R_2(0) = 1.7$ (dashed lines) and $R_1(0) = 1.3$, $R_2(0) = 2.2$ (dot-dashed lines).

FIG. 24. Evolution of a quasi-static drop profile for an axisymmetric annular drop in the case of zero gravity when $J_0 = 1$, $V_0 = 0.1696$, with the initial conditions $R_1(0) = 1.3$, $R_2(0) = 1.7$.

FIG. 25. Evolution of a quasi-static drop profile for an axisymmetric annular drop in the case of zero gravity when $J_0 = 1$, $V_0 = 0.1696$, with the initial conditions $R_1(0) = 1.3$, $R_2(0) = 2.2$.

FIG. 26. Plot of D_2 defined in Eq. (A3) as a function of c.

FIG. 27. Plot of λ_+ and λ_- for $c = 10$, 15, 25 and 35. The dots ($\bullet$) denote the points corresponding to $\lambda_{\min}$ and $\lambda_{\max}$.

FIG. 28. Plot of $\lambda_{\min}$ (upper curve) and $\lambda_{\max}$ (lower curve) as a function of c.

Fig. 1

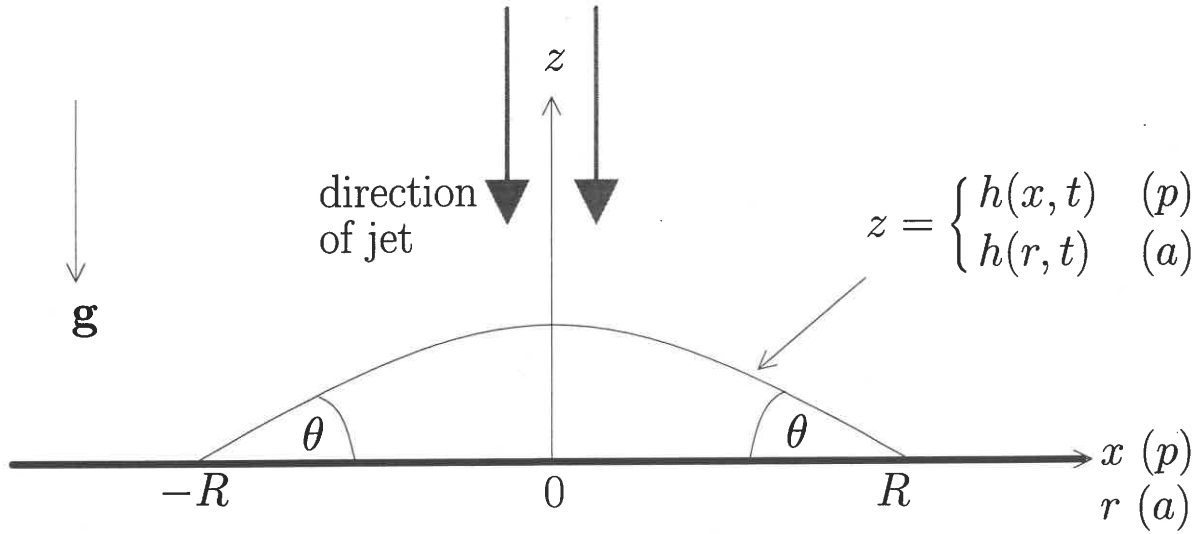
z
direction
of jet
g
$z = \begin{cases} h(x,t) & (p) \\ h(r,t) & (a) \end{cases}$
θ
θ
−R
0
R
x (p)
r (a)

Fig. 2

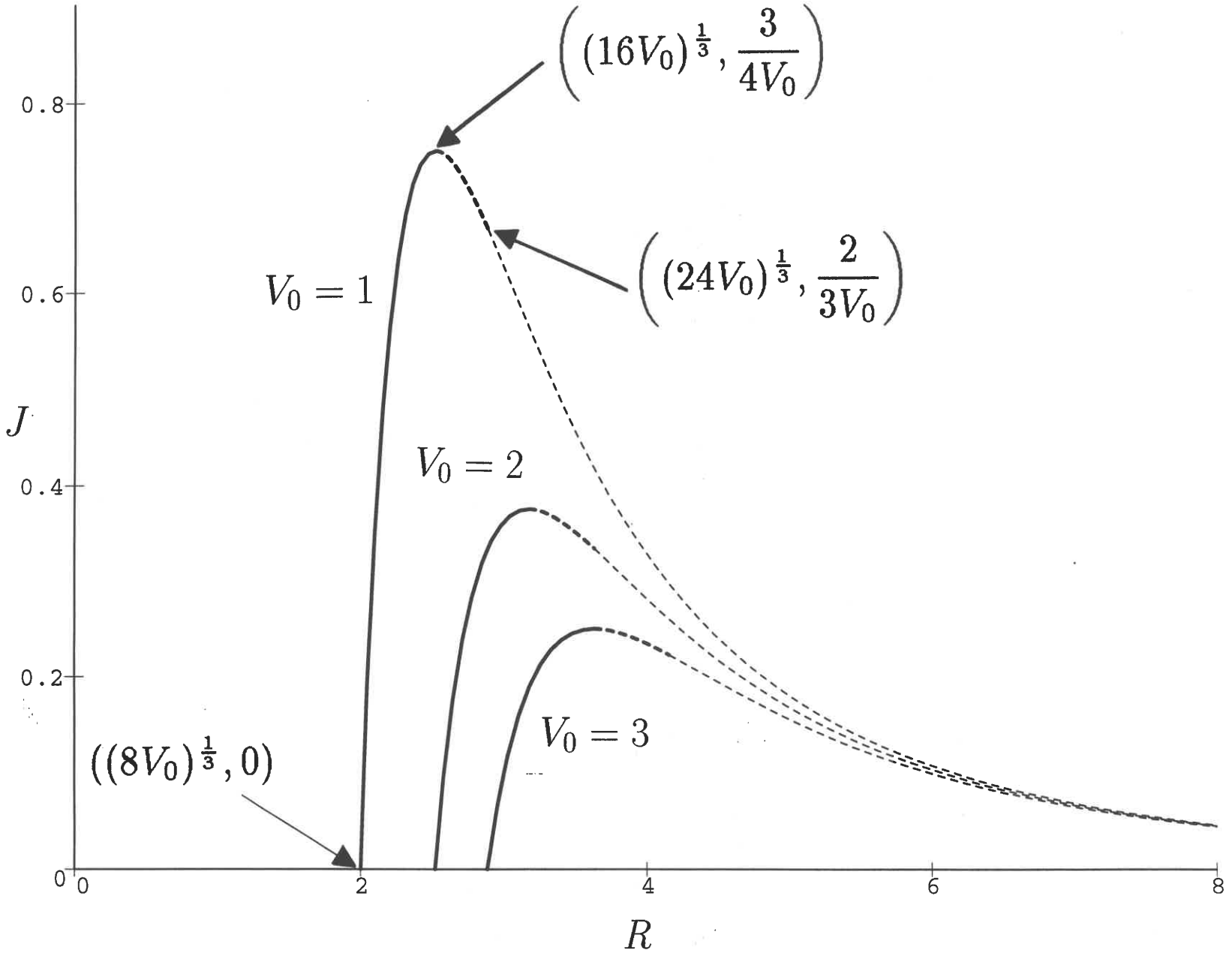
$\left((16V_0)^{\frac{1}{3}}, \frac{3}{4V_0}\right)$
$\left((24V_0)^{\frac{1}{3}}, \frac{2}{3V_0}\right)$
$V_0 = 1$
$V_0 = 2$
$V_0 = 3$
$((8V_0)^{\frac{1}{3}}, 0)$
0.8
0.6
0.4
0.2
0
J
0
2
4
6
8
R

Fig. 3

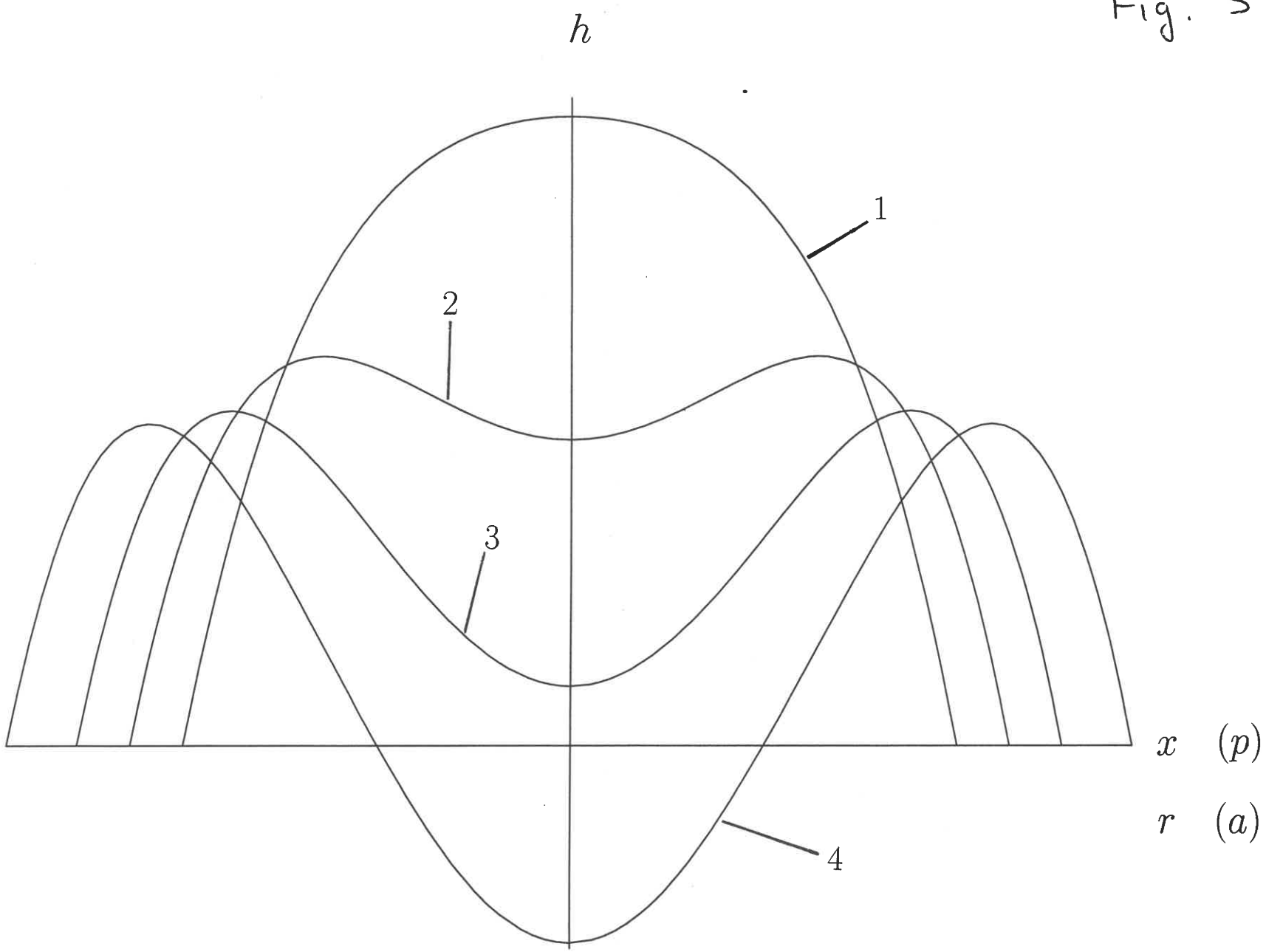

Fig. 4

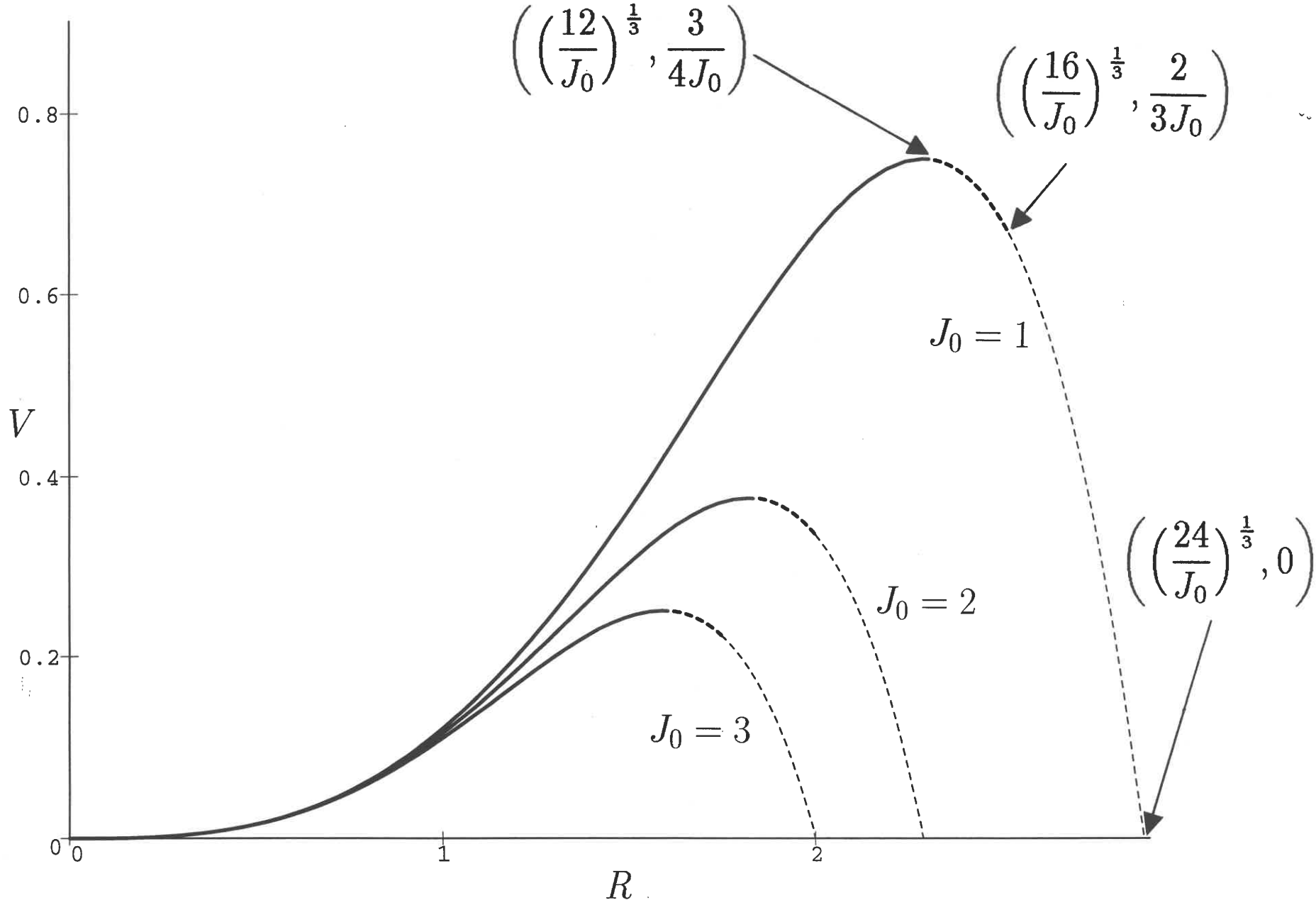
$\left(\left(\frac{12}{J_0}\right)^{\frac{1}{3}}, \frac{3}{4J_0}\right)$
$\left(\left(\frac{16}{J_0}\right)^{\frac{1}{3}}, \frac{2}{3J_0}\right)$
$\left(\left(\frac{24}{J_0}\right)^{\frac{1}{3}}, 0\right)$
$J_0 = 1$
$J_0 = 2$
$J_0 = 3$
0.8
0.6
0.4
0.2
0
V
0
1
2
R

Fig. 5

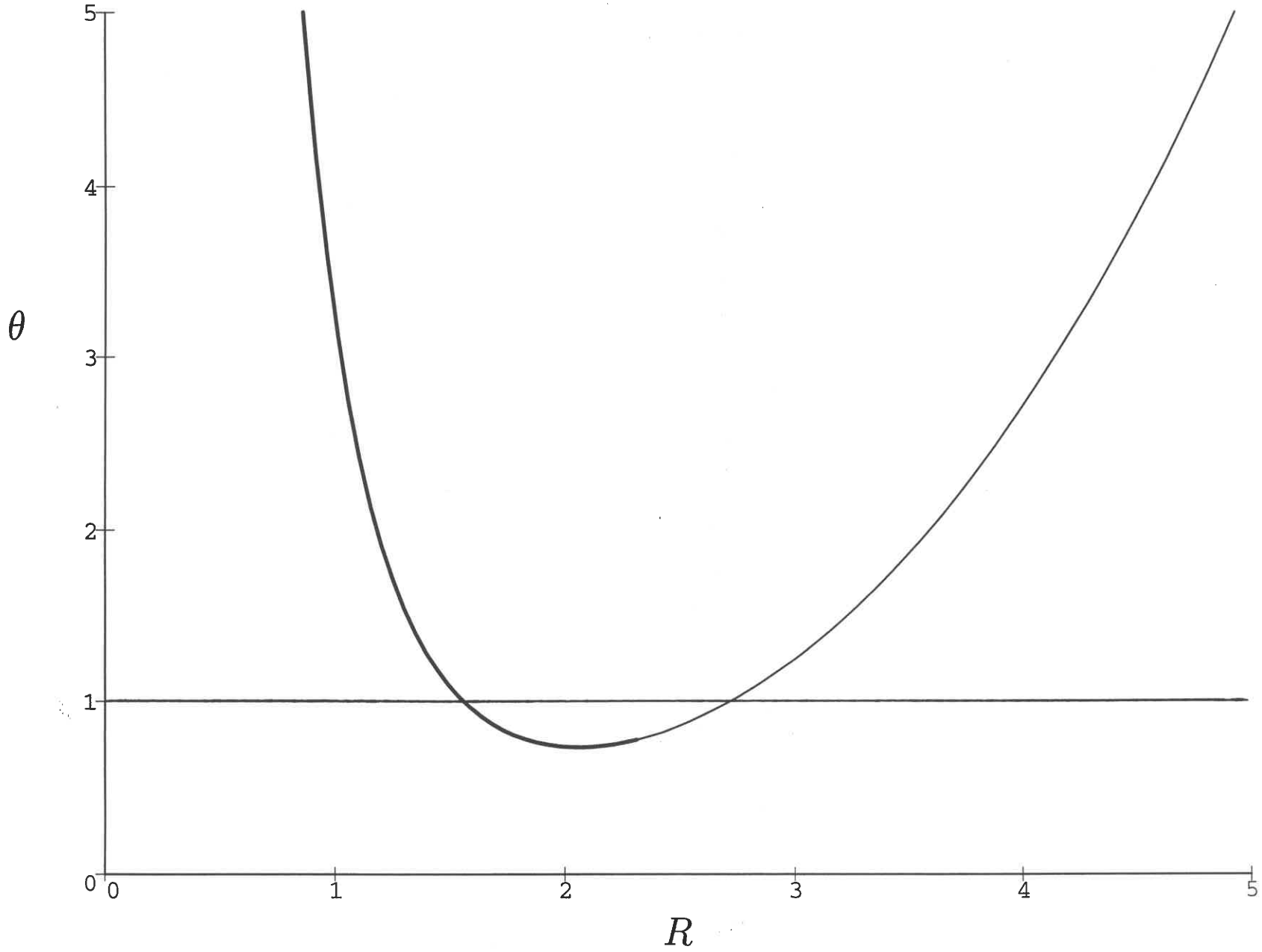

Fig. 6

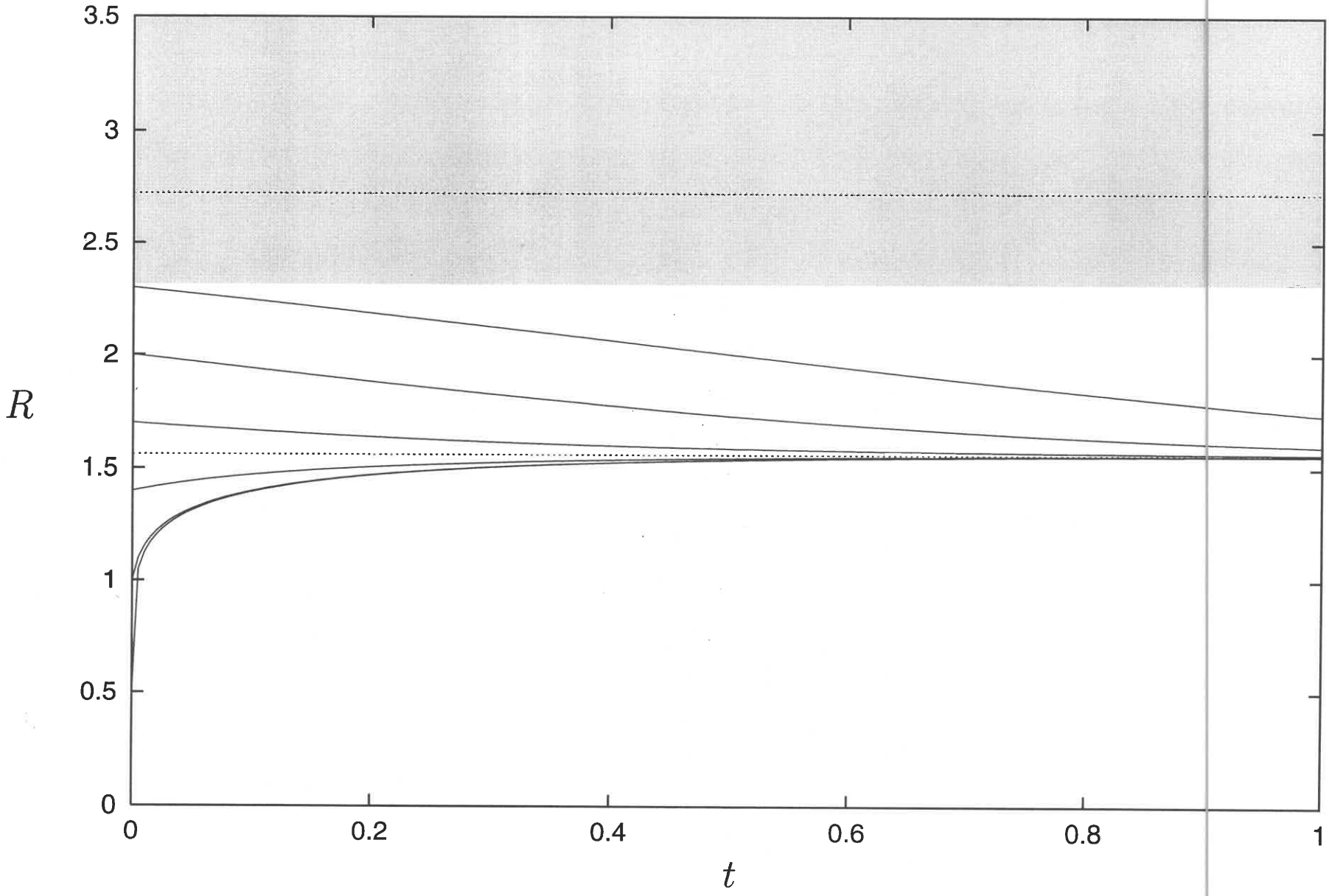

Fig. 7

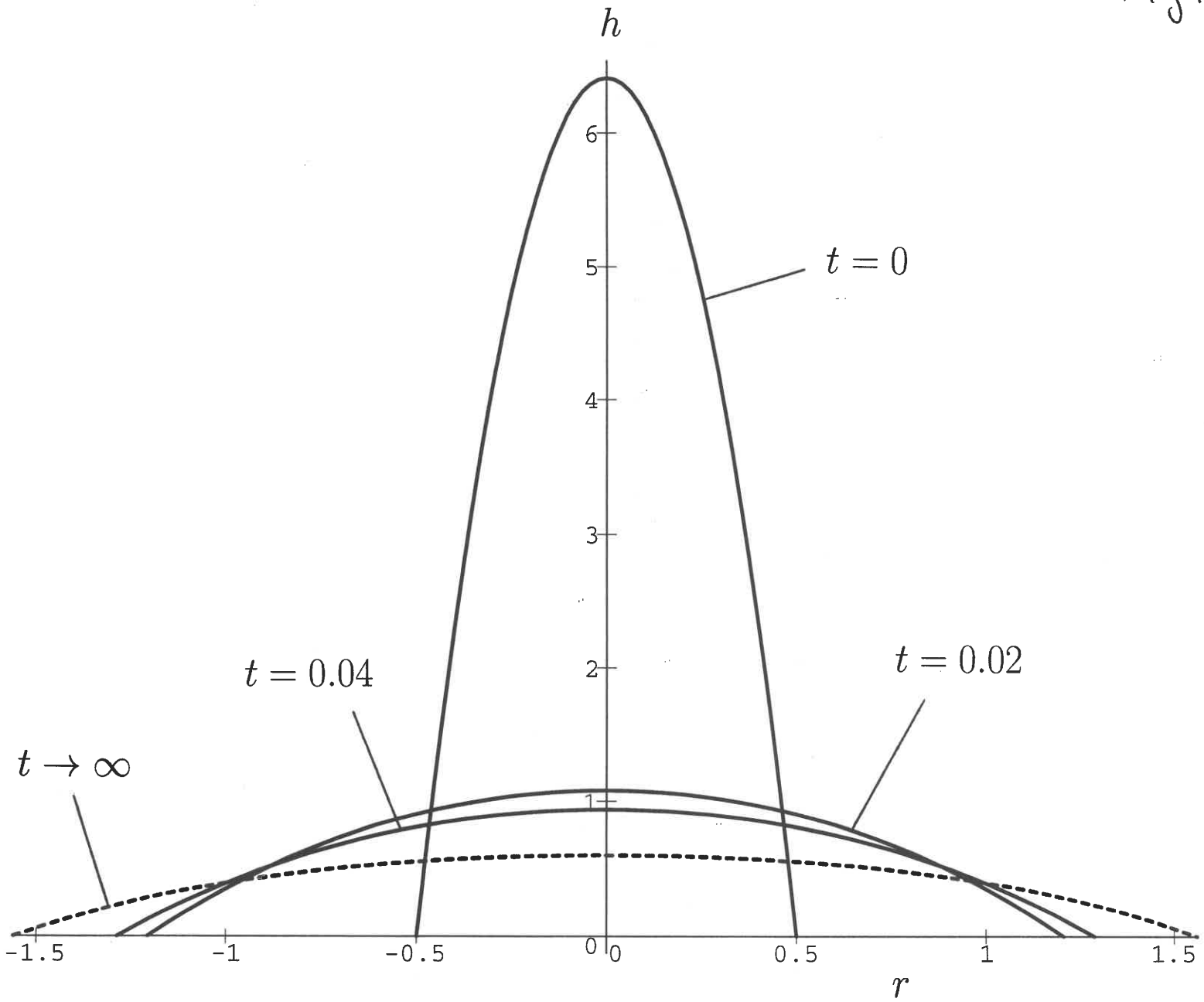

Fig. 8

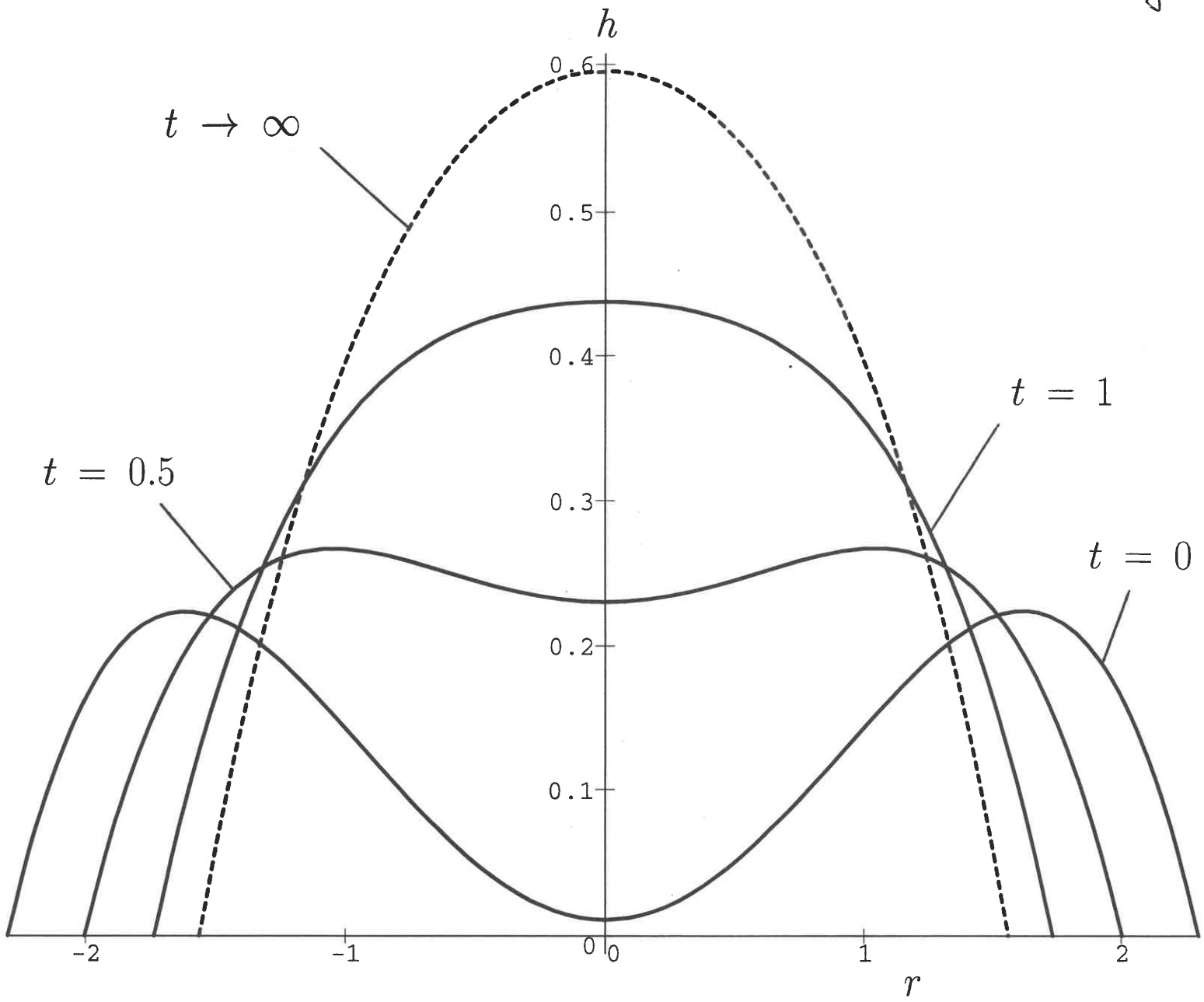

Fig. 9

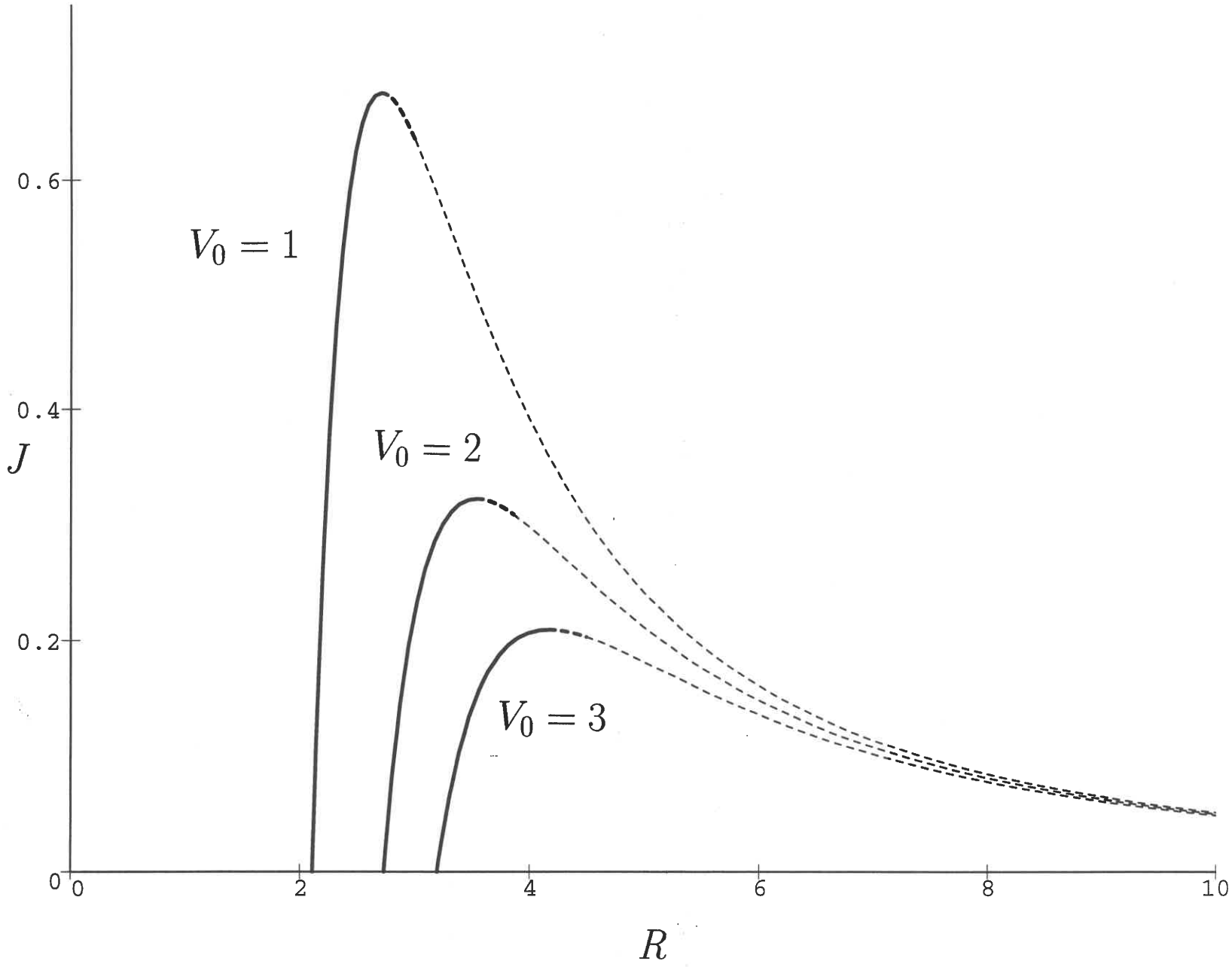

Fig. 10

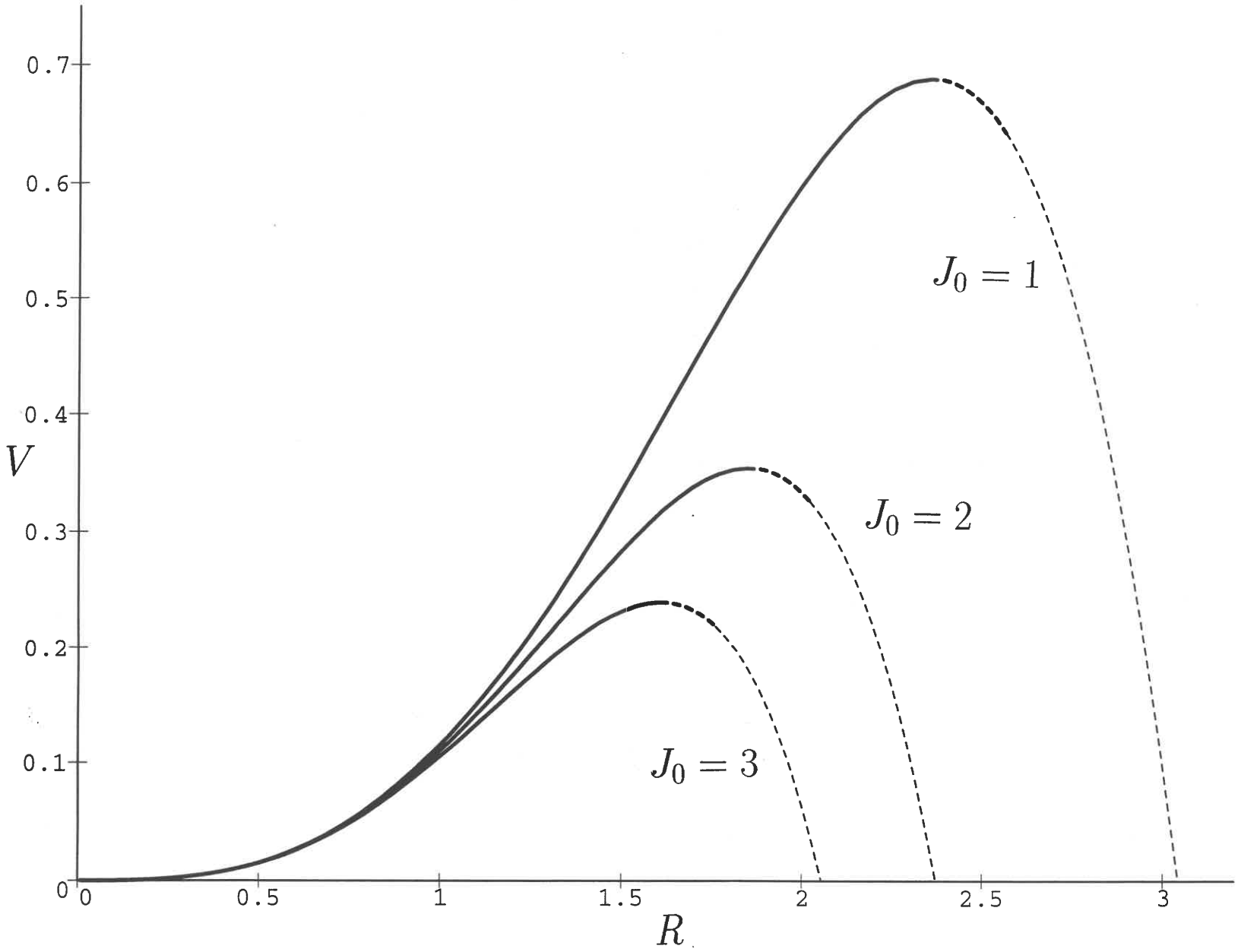

Fig. 11(a)

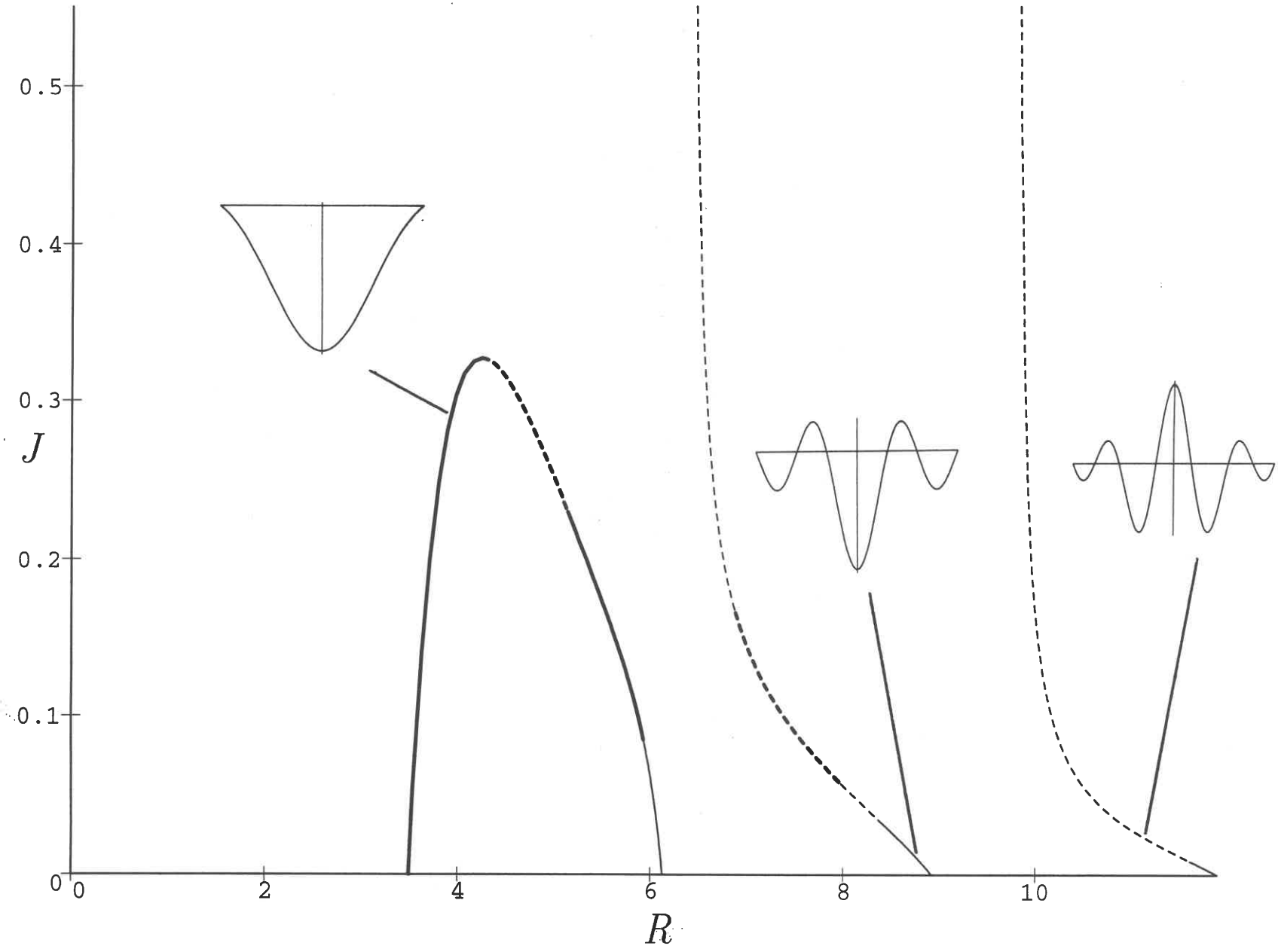

Fig. 11 (b)

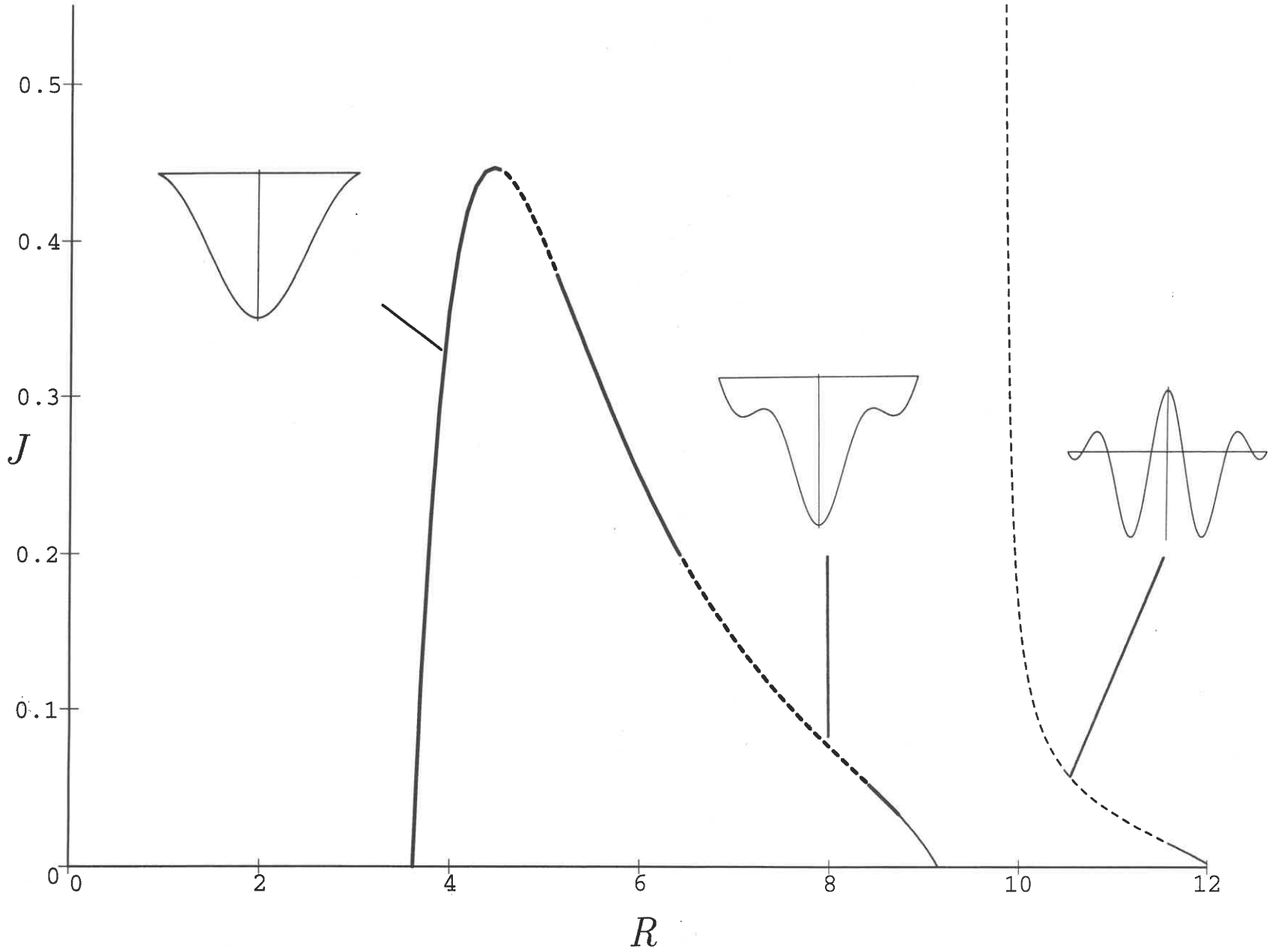

Fig. 11(c)

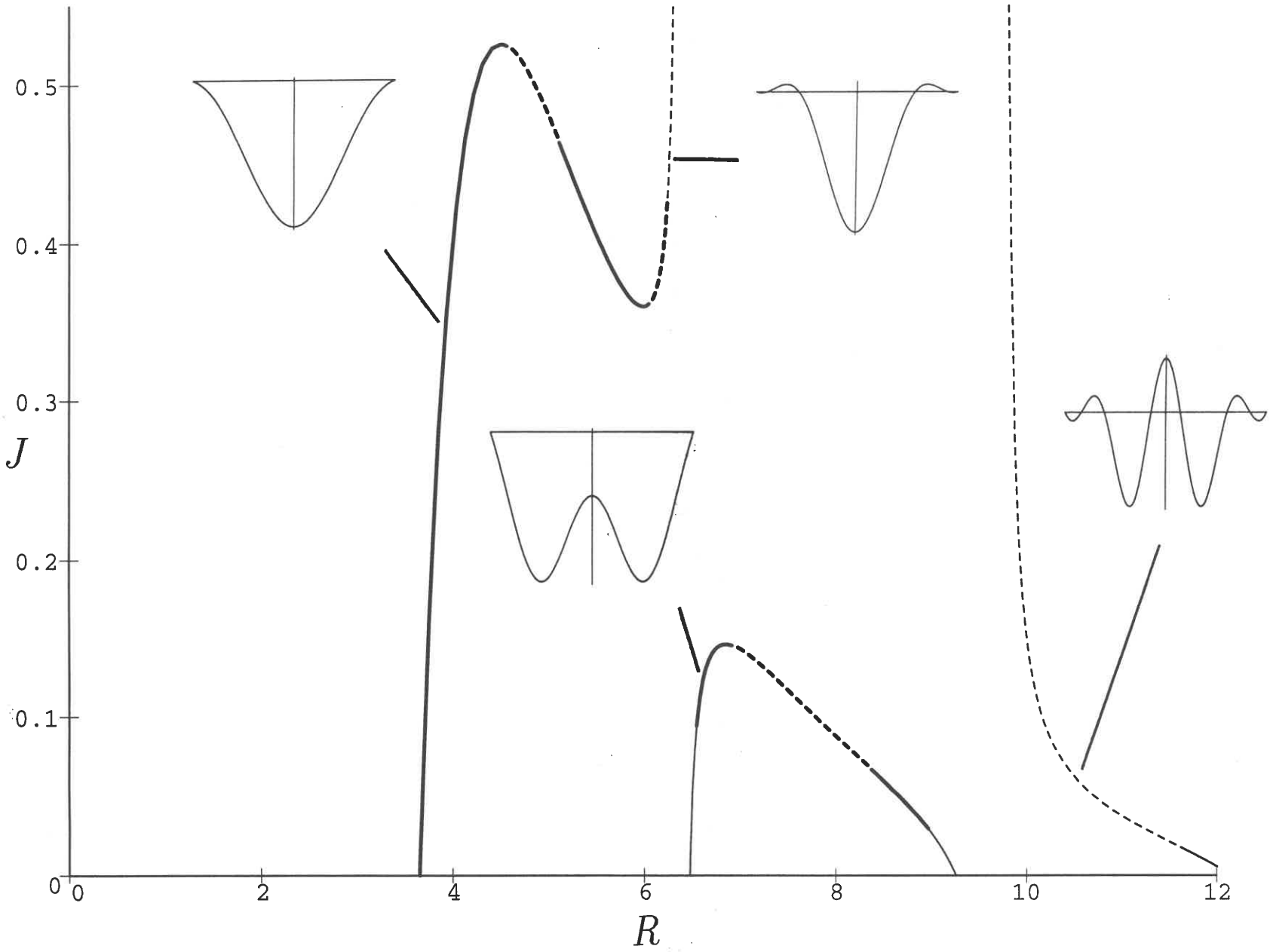

Fig. 12 (a)

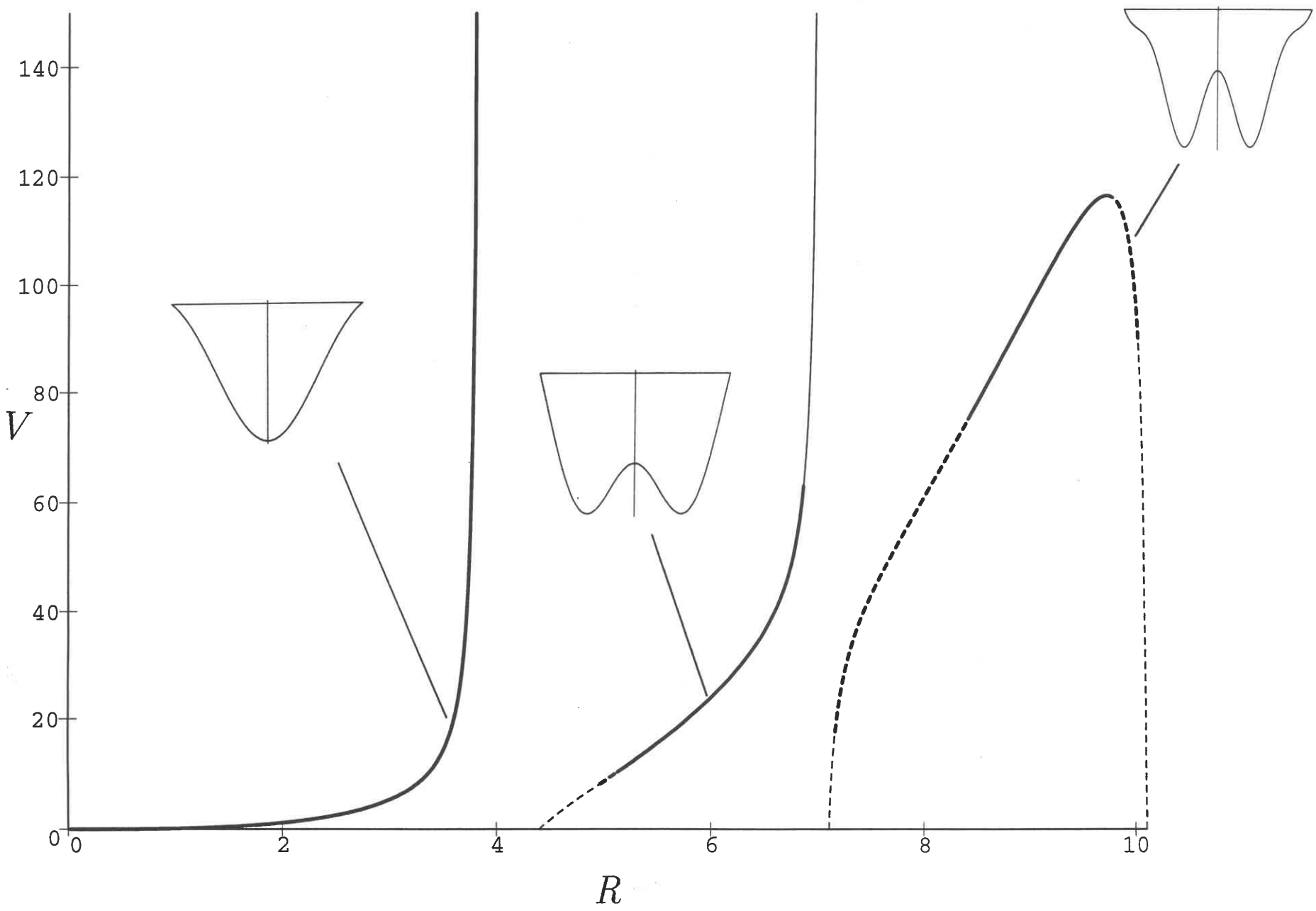

Fig. 12(b)

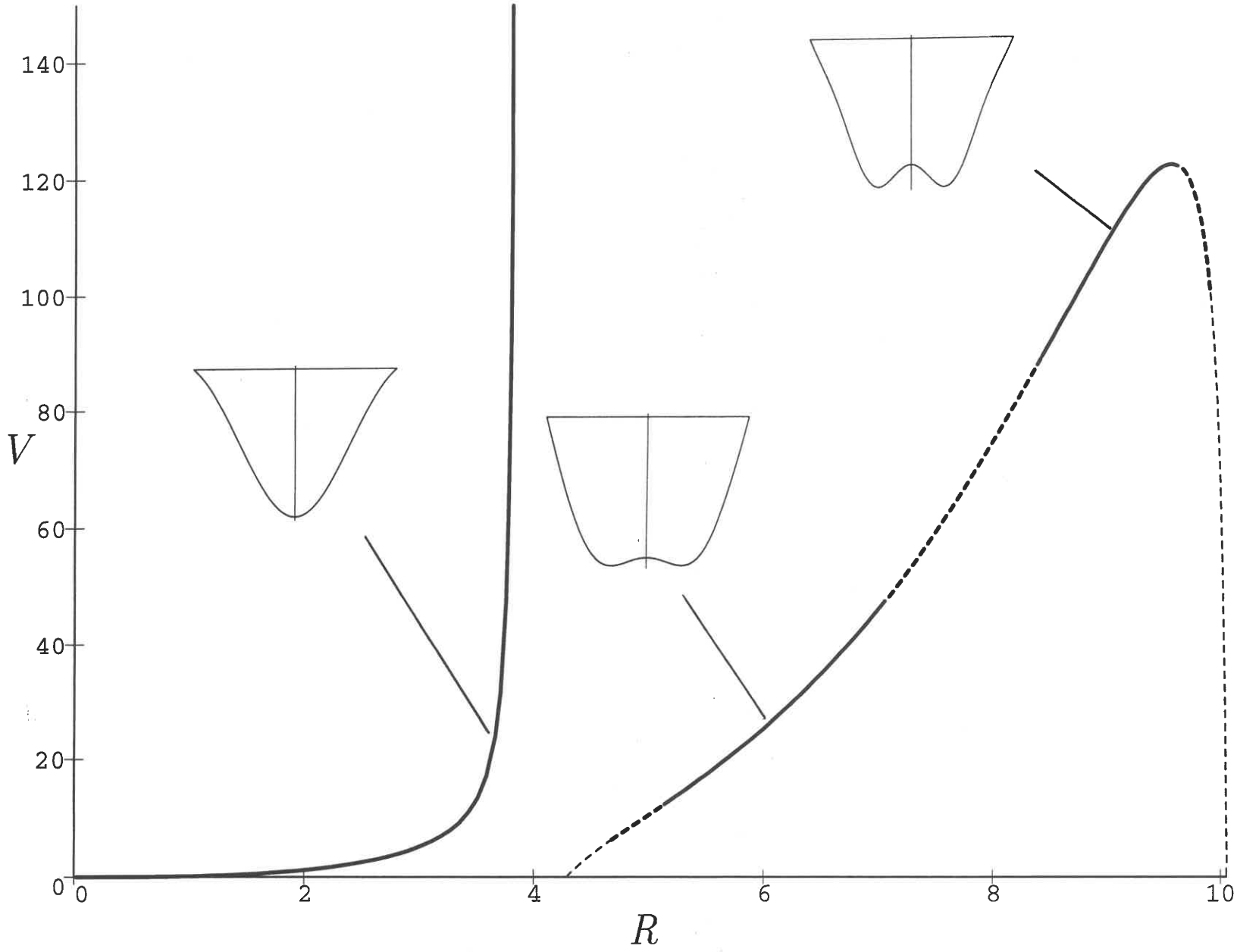

Fig. 12(c)

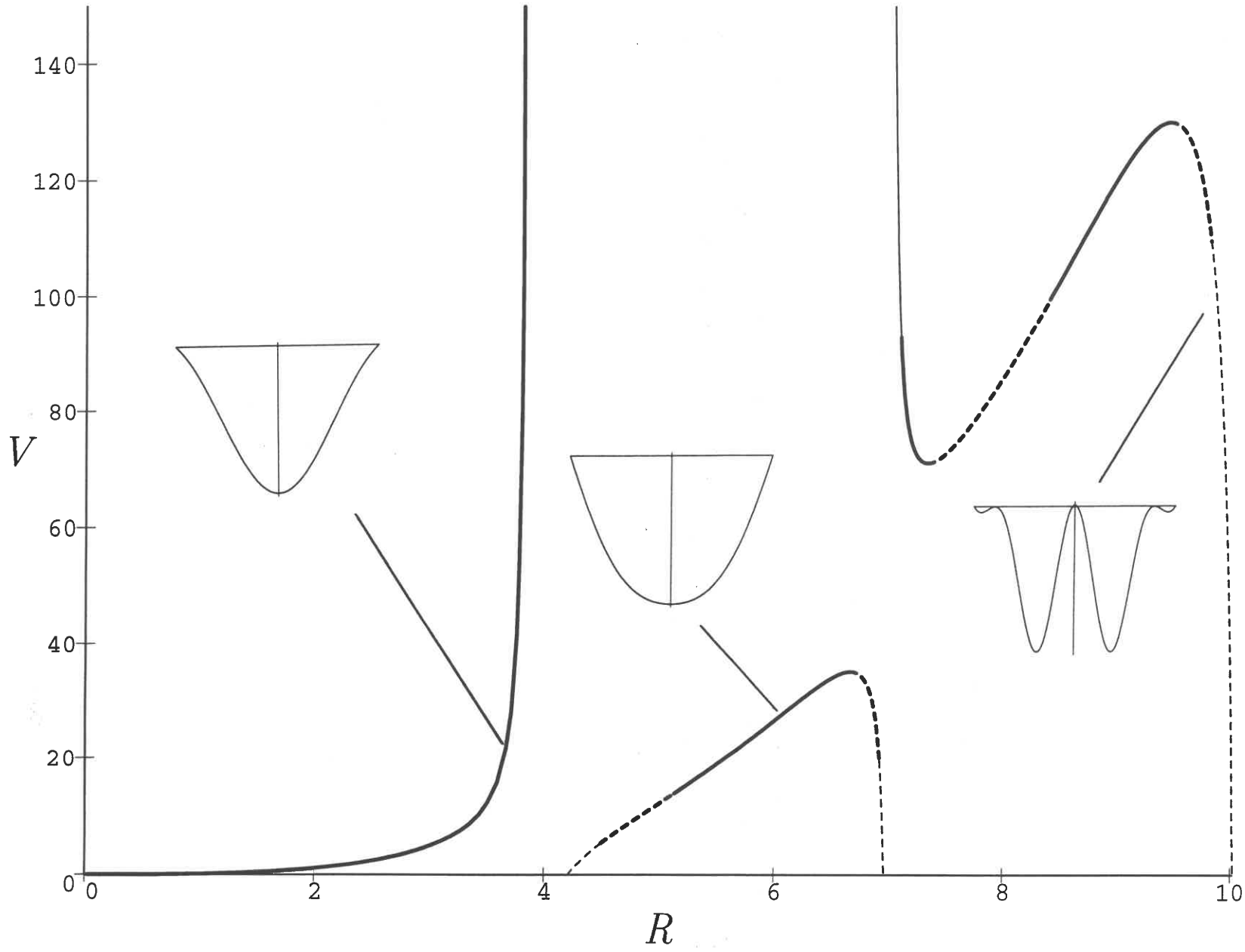

Fig. 13

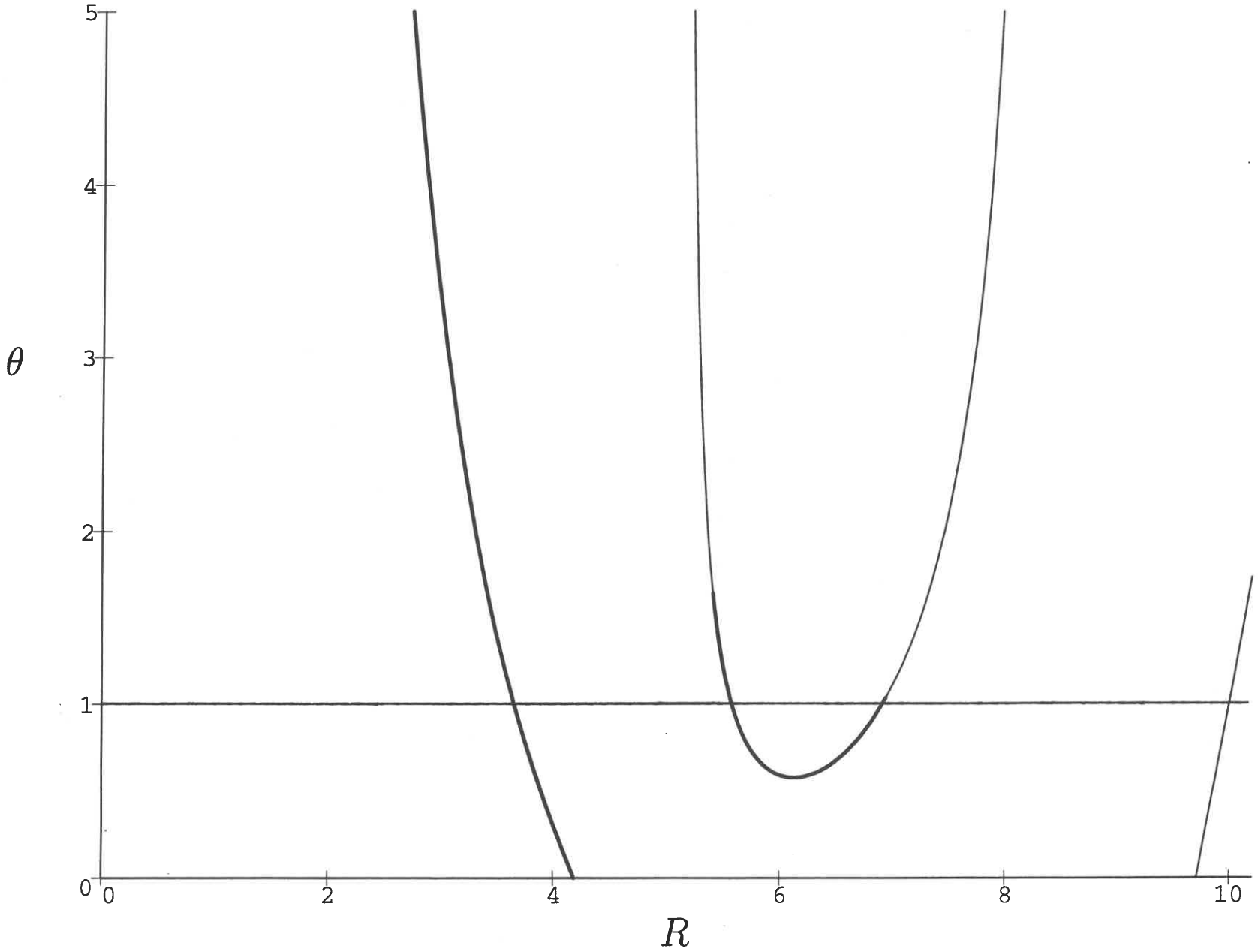

Fig. 14

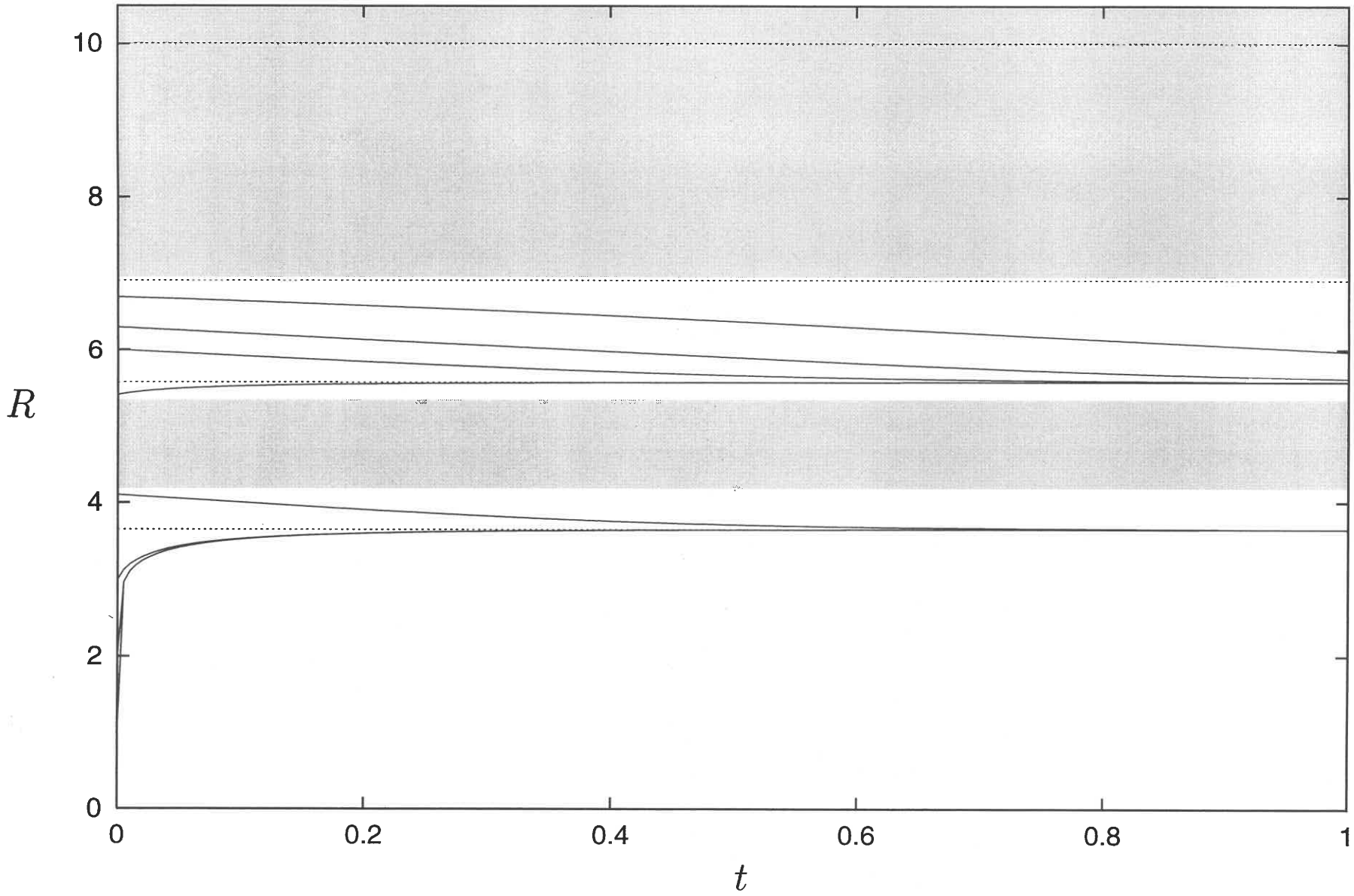

Fig. 15

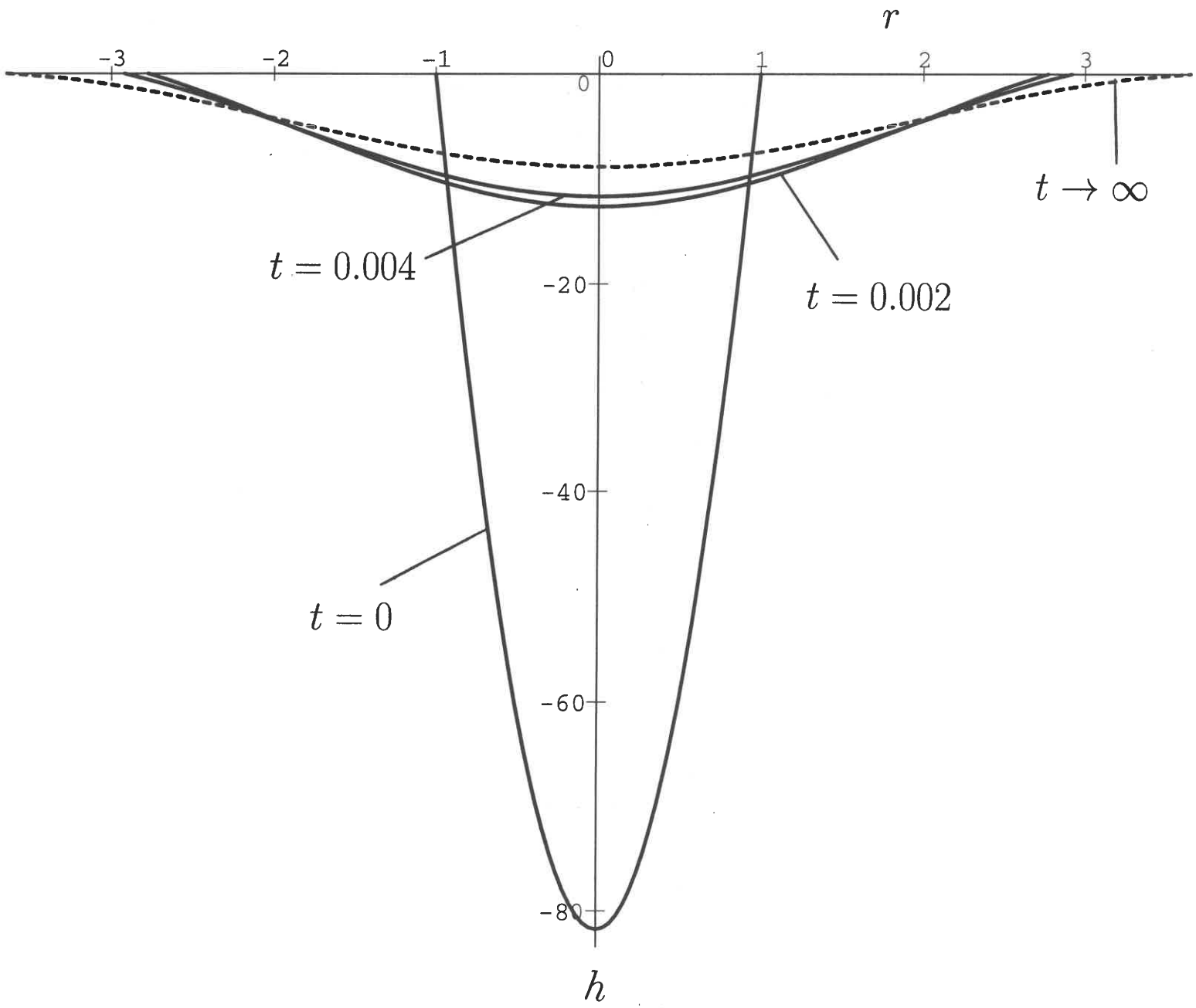

Fig. 16

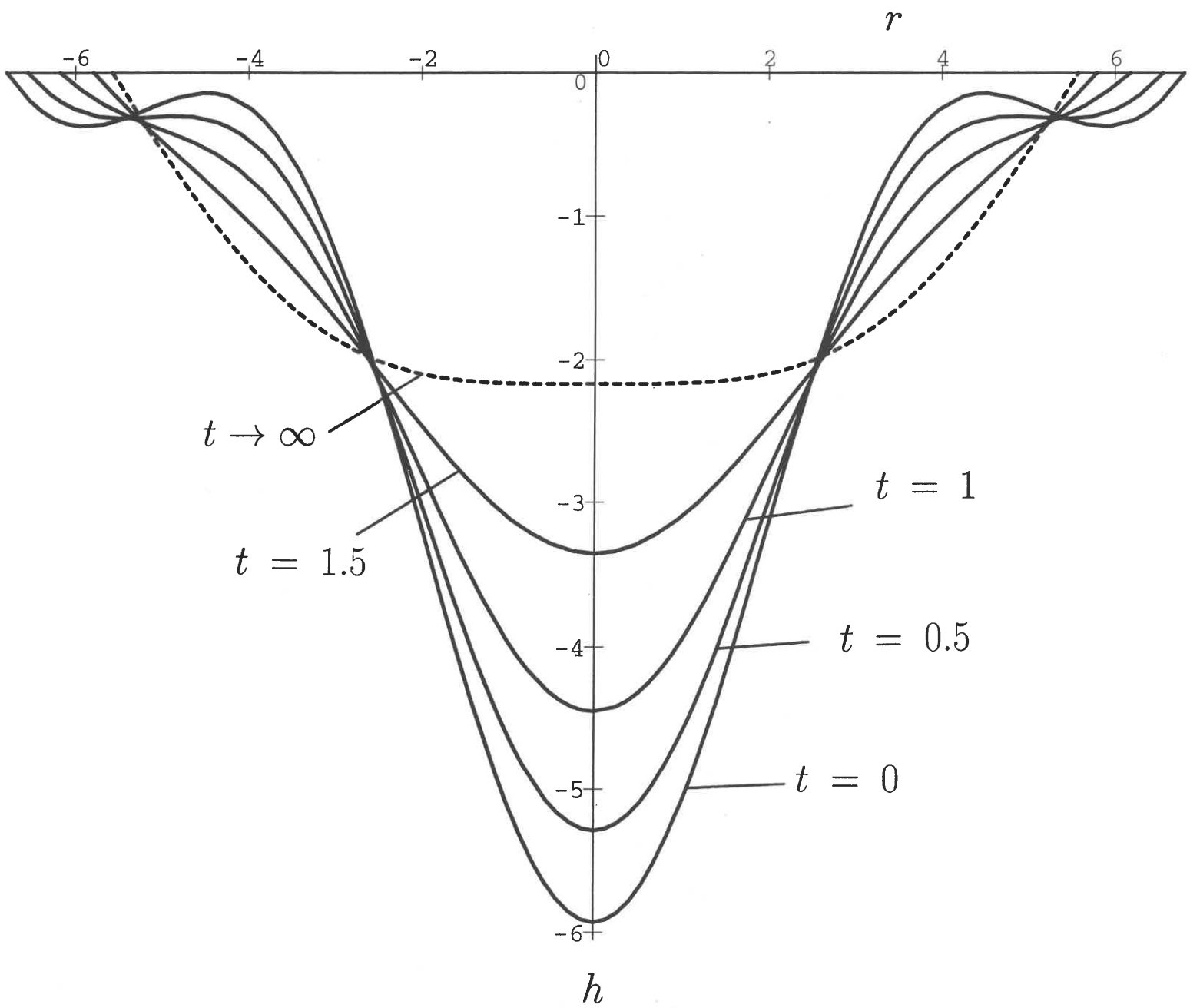

Fig. 17

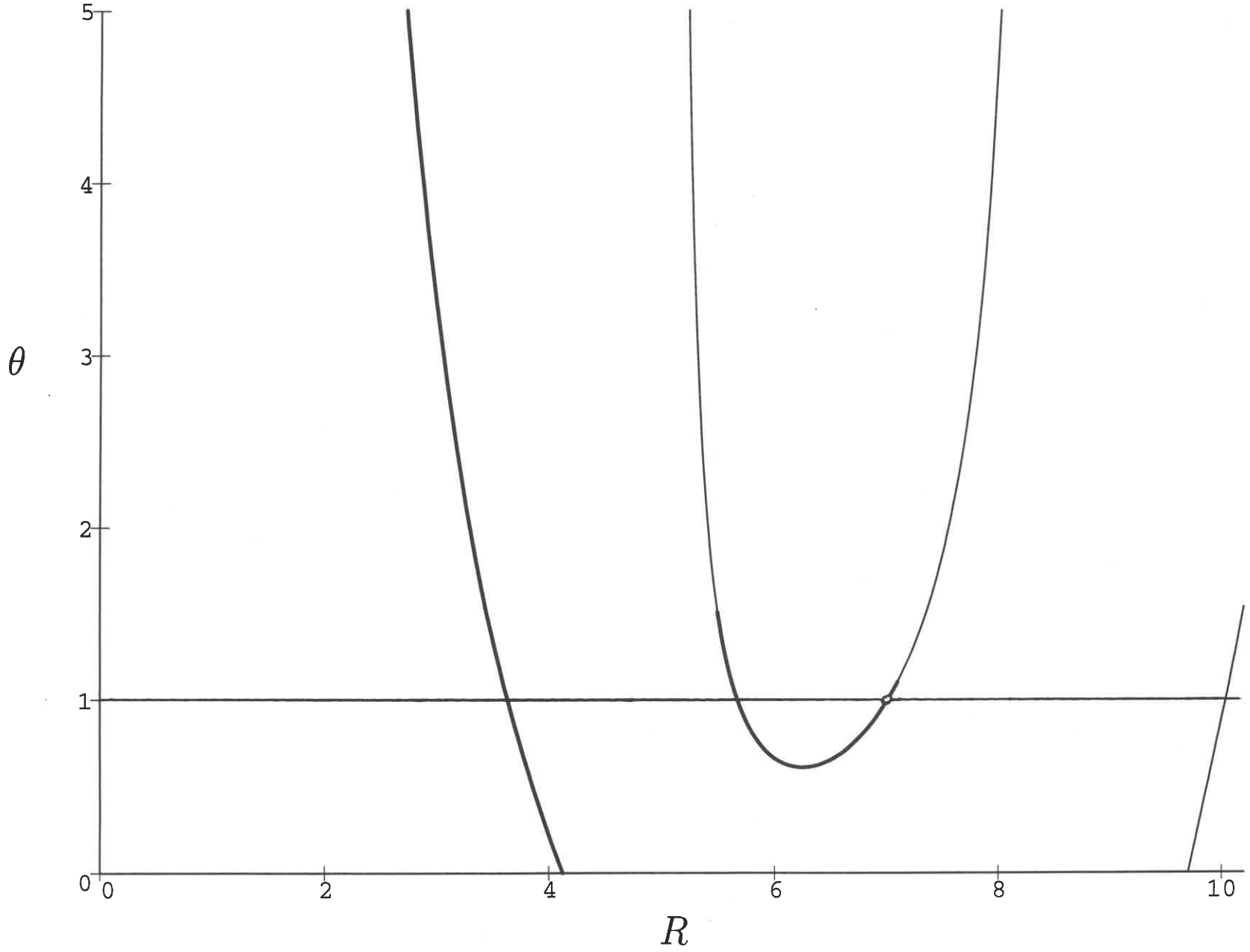

Fig. 18

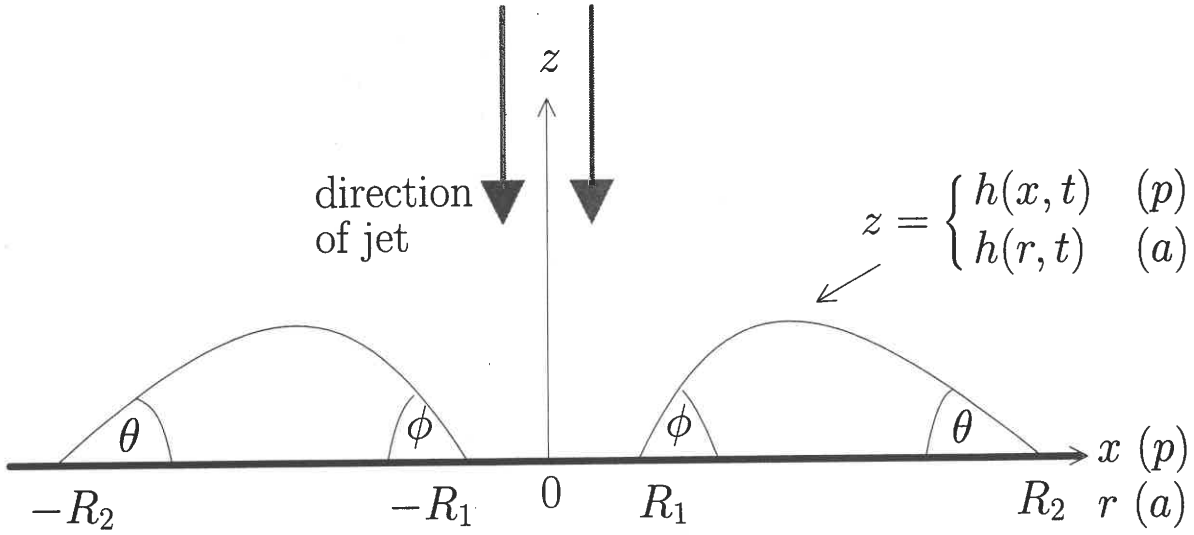
z
direction
of jet
$z = \begin{cases} h(x,t) & (p) \\ h(r,t) & (a) \end{cases}$
θ
ϕ
ϕ
θ
x (p)
r (a)
$-R_2$
$-R_1$
0
R_1
R_2

Fig. 19

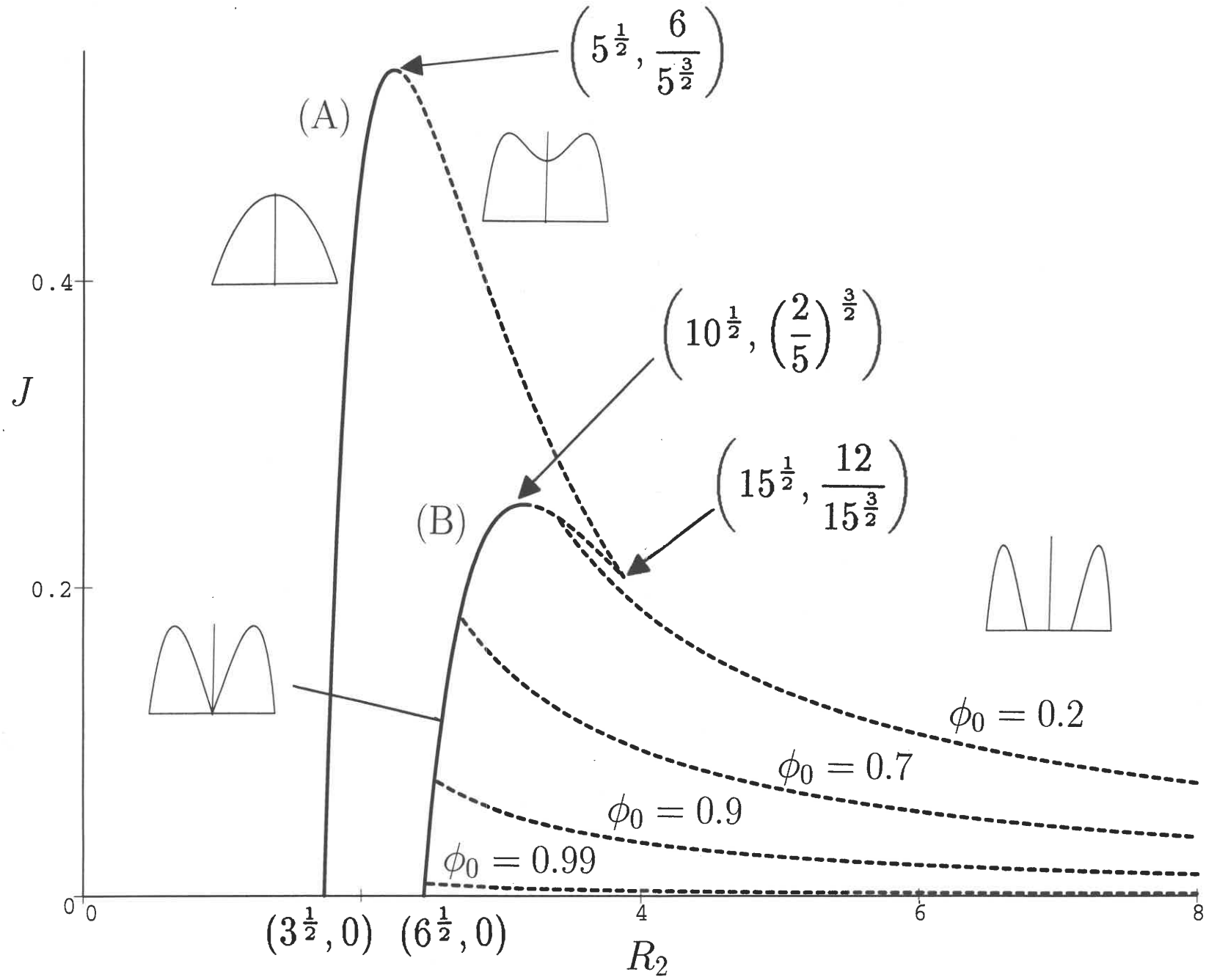
$\left(5^{\frac{1}{2}}, \frac{6}{5^{\frac{3}{2}}}\right)$
(A)
$\left(10^{\frac{1}{2}}, \left(\frac{2}{5}\right)^{\frac{3}{2}}\right)$
$\left(15^{\frac{1}{2}}, \frac{12}{15^{\frac{3}{2}}}\right)$
(B)
$\phi_0 = 0.2$
$\phi_0 = 0.7$
$\phi_0 = 0.9$
$\phi_0 = 0.99$
0.4
0.2
0
J
0
4
6
8
$(3^{\frac{1}{2}}, 0)$
$(6^{\frac{1}{2}}, 0)$
R_2

Fig. 20

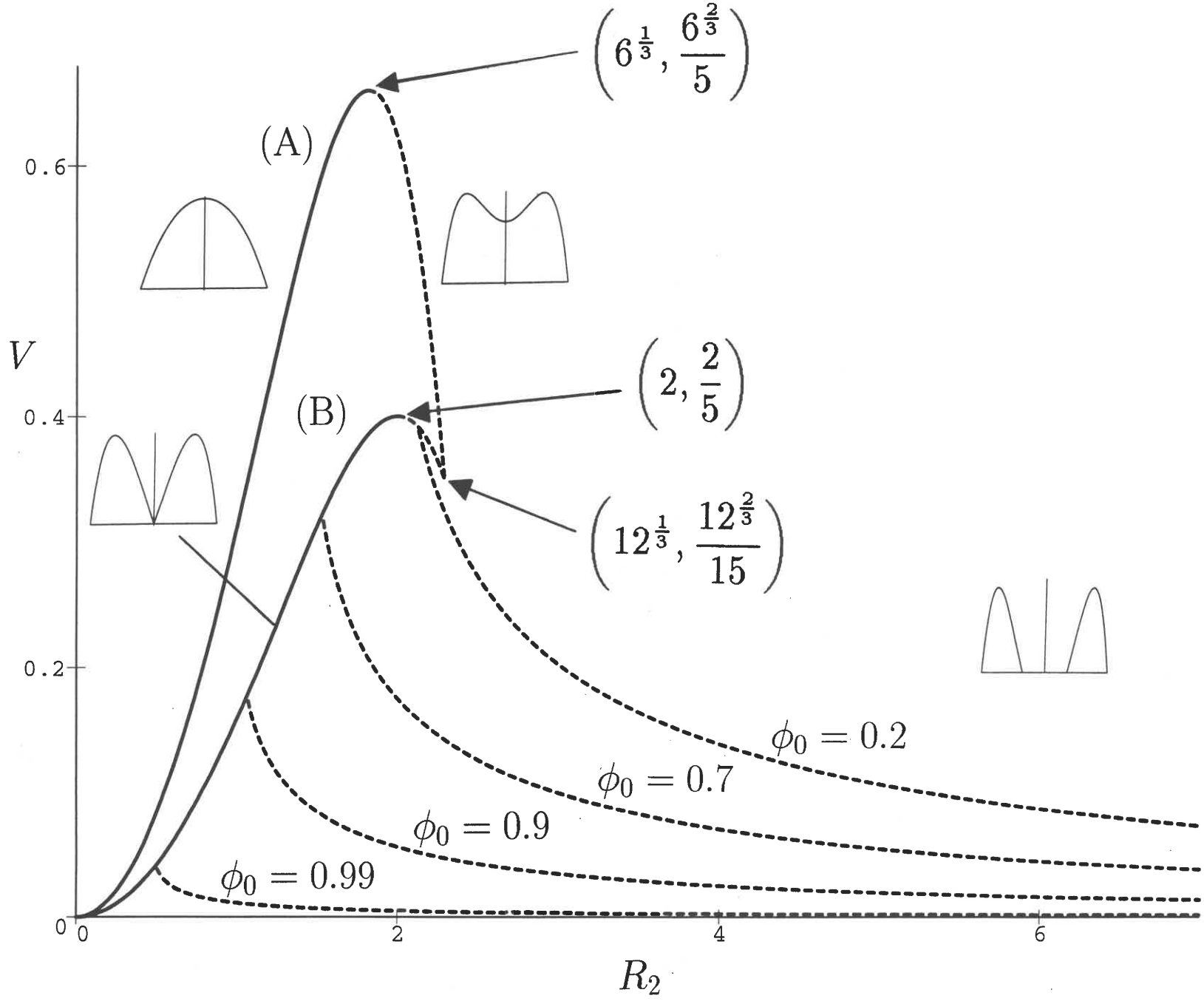
$\left(6^{\frac{1}{3}}, \frac{6^{\frac{2}{3}}}{5}\right)$
(A)
0.6
V
0.4
(B)
$\left(2, \frac{2}{5}\right)$
$\left(12^{\frac{1}{3}}, \frac{12^{\frac{2}{3}}}{15}\right)$
0.2
$\phi_0 = 0.2$
$\phi_0 = 0.7$
$\phi_0 = 0.9$
$\phi_0 = 0.99$
0
0
2
4
6
R_2

Fig. 21

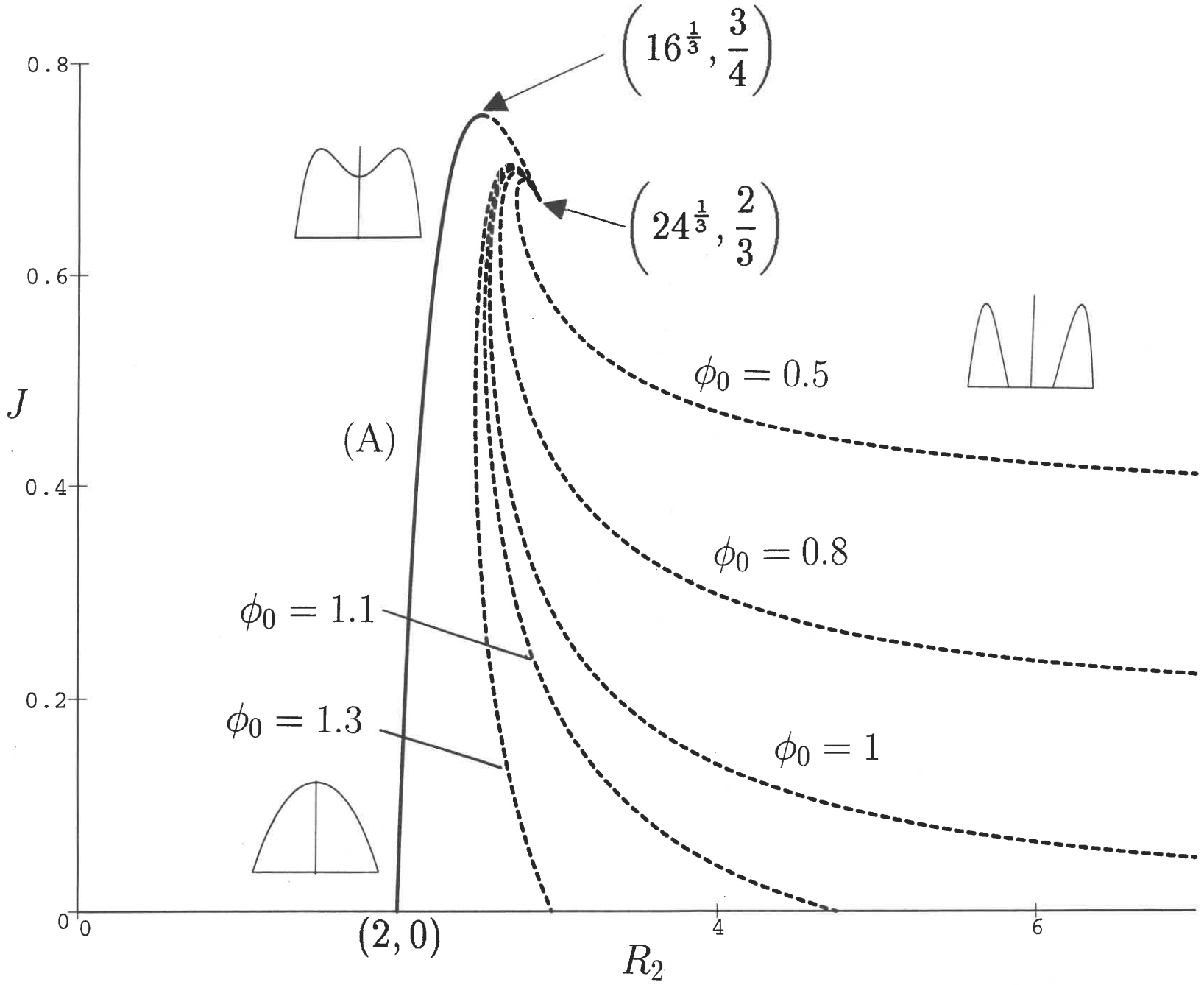
$\left(16^{\frac{1}{3}}, \frac{3}{4}\right)$
$\left(24^{\frac{1}{3}}, \frac{2}{3}\right)$
$\phi_0 = 0.5$
$\phi_0 = 0.8$
$\phi_0 = 1$
$\phi_0 = 1.1$
$\phi_0 = 1.3$
(A)
J
R_2
0.8
0.6
0.4
0.2
0
0
4
6
(2, 0)

Fig. 22

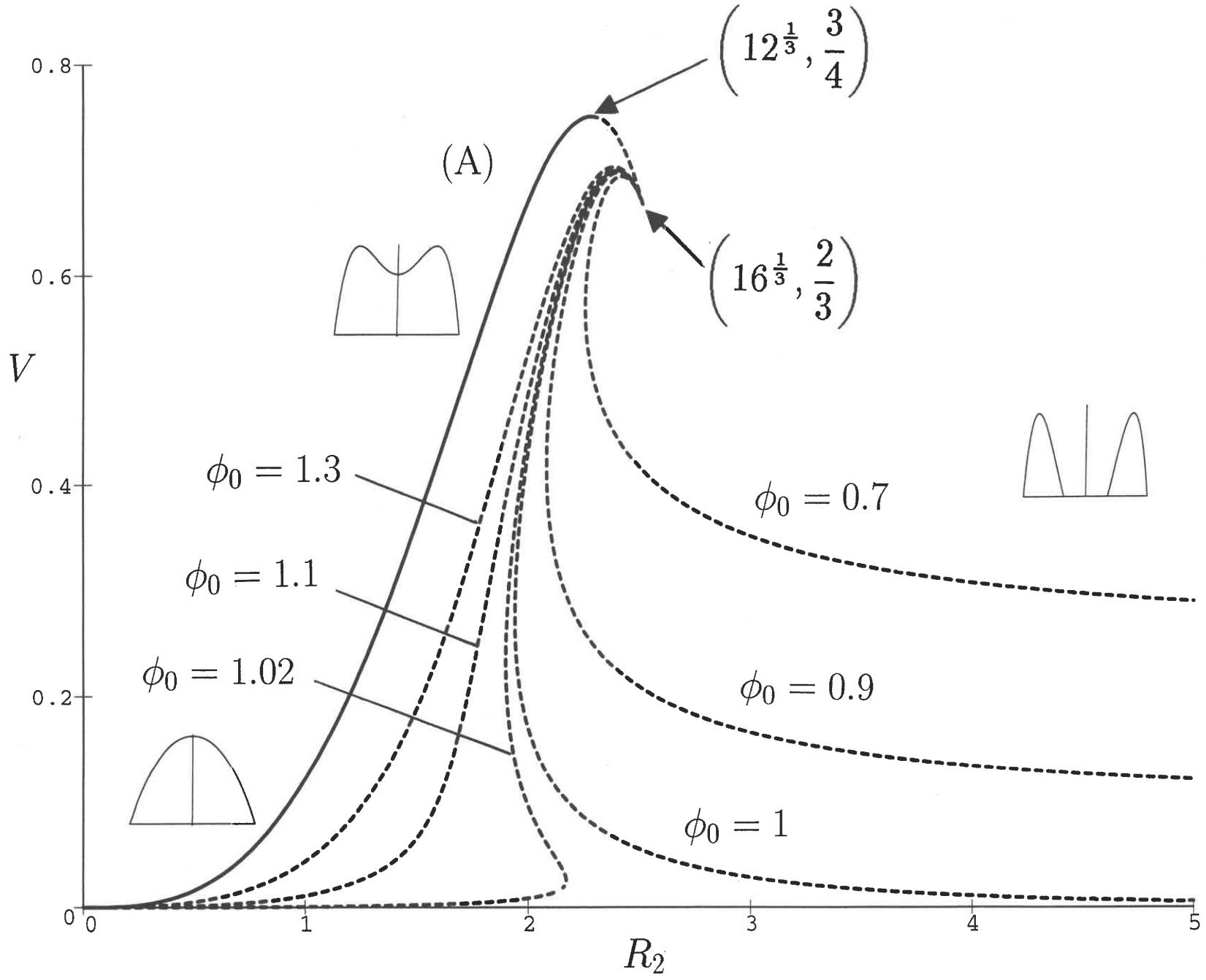
$\left(12^{\frac{1}{3}}, \frac{3}{4}\right)$
(A)
$\left(16^{\frac{1}{3}}, \frac{2}{3}\right)$
$\phi_0 = 1.3$
$\phi_0 = 1.1$
$\phi_0 = 1.02$
$\phi_0 = 0.7$
$\phi_0 = 0.9$
$\phi_0 = 1$
V
R_2
0.8
0.6
0.4
0.2
0
0
1
2
3
4
5

Fig. 23

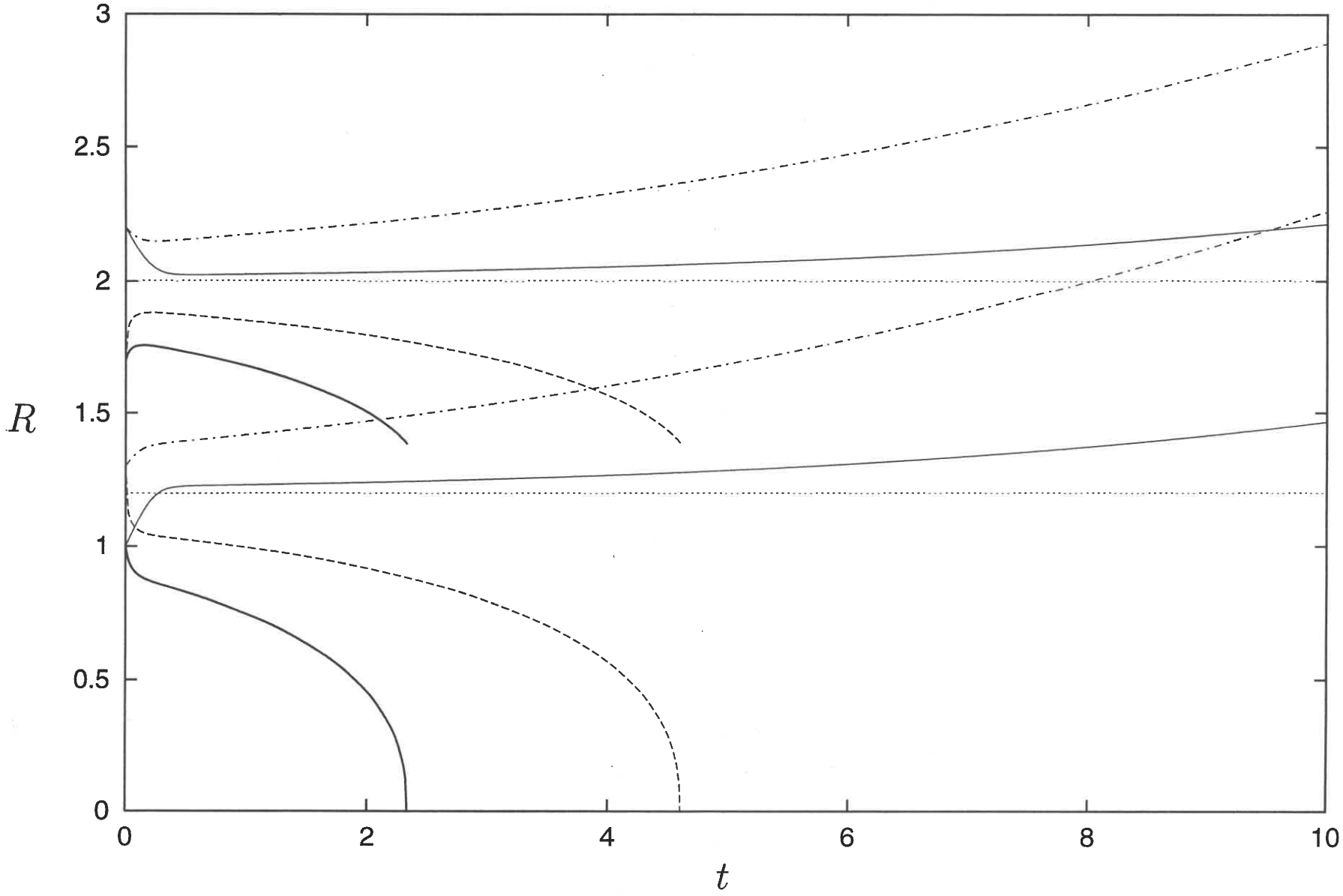

Fig. 24

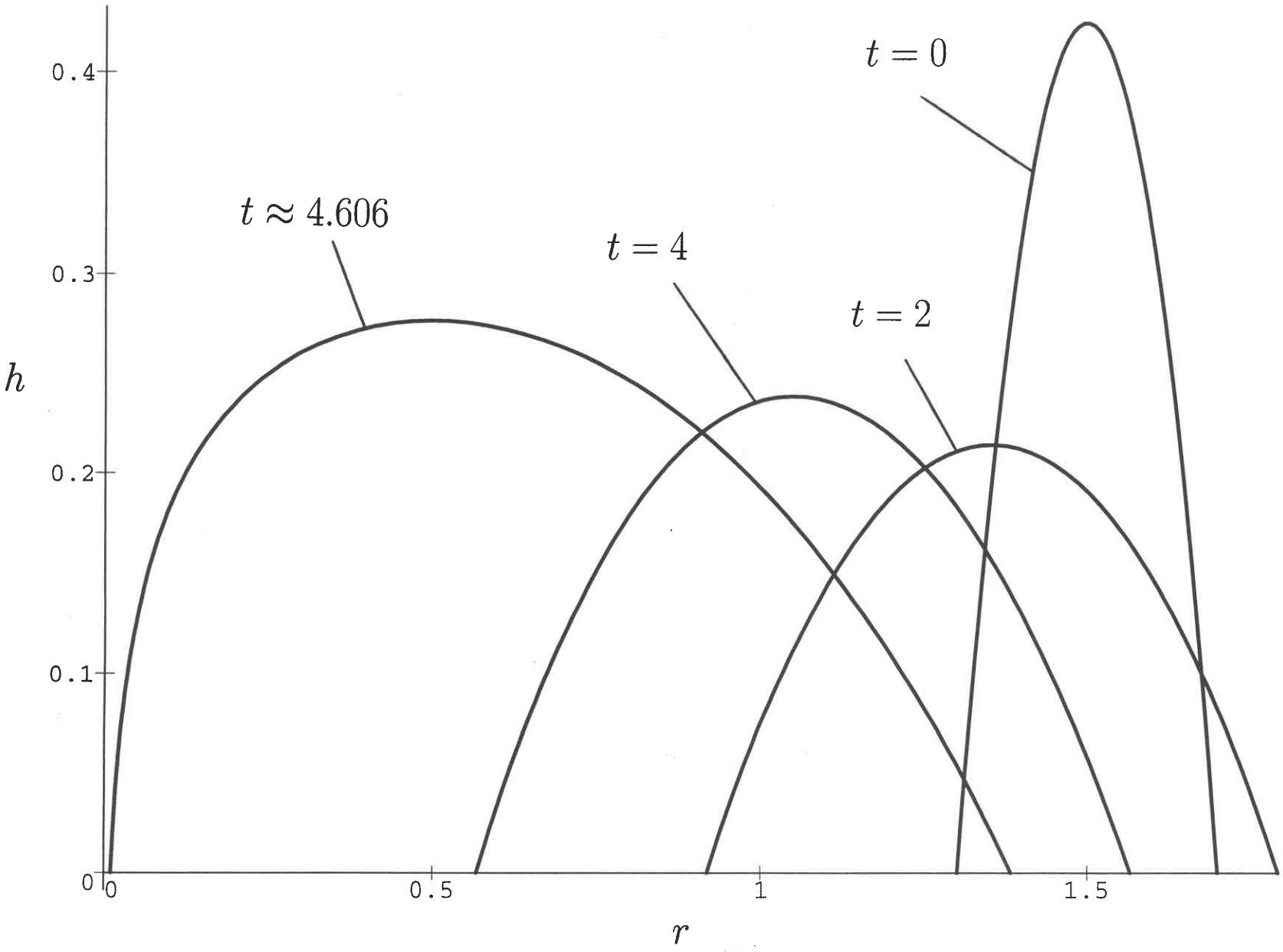

Fig. 25

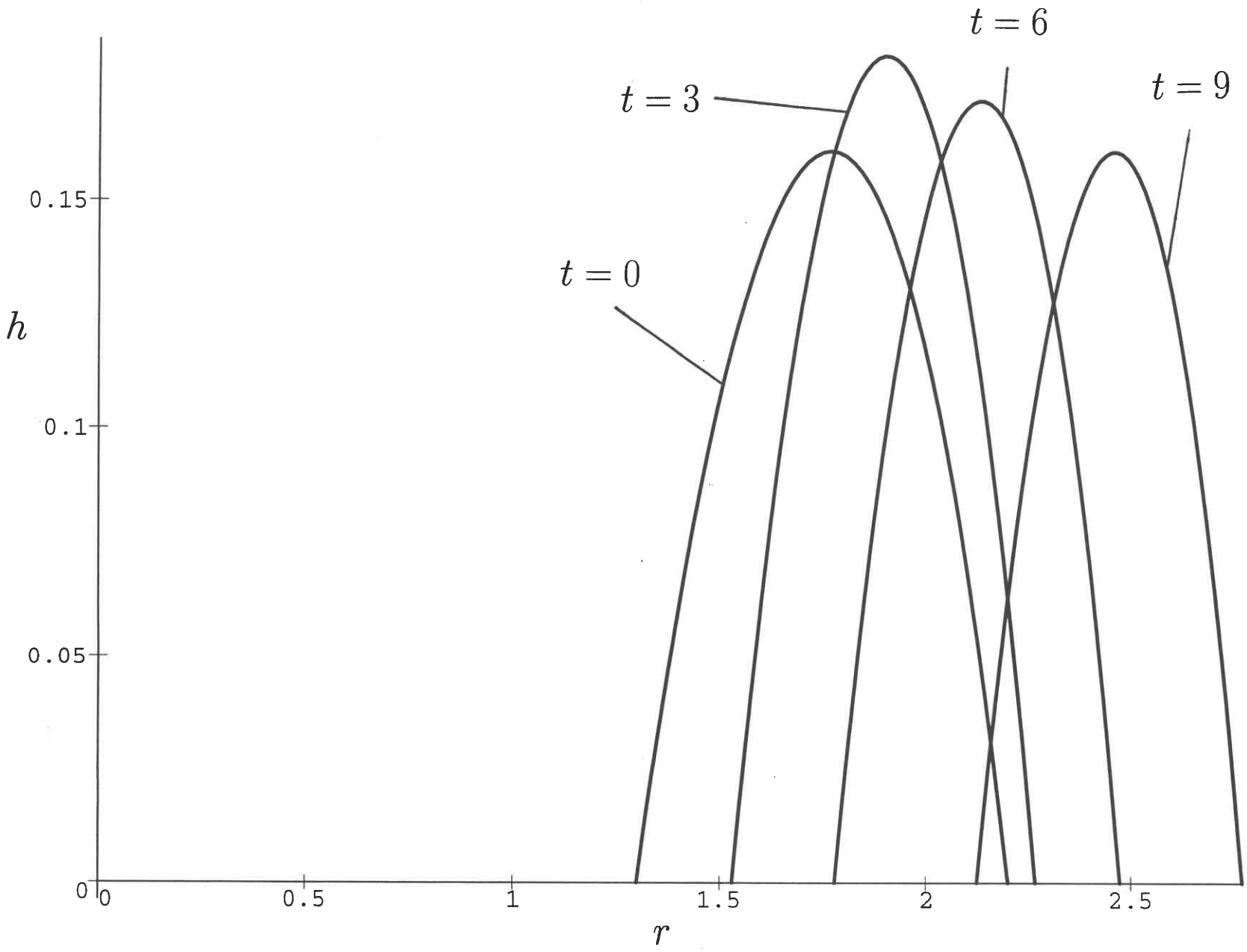

Fig. 26

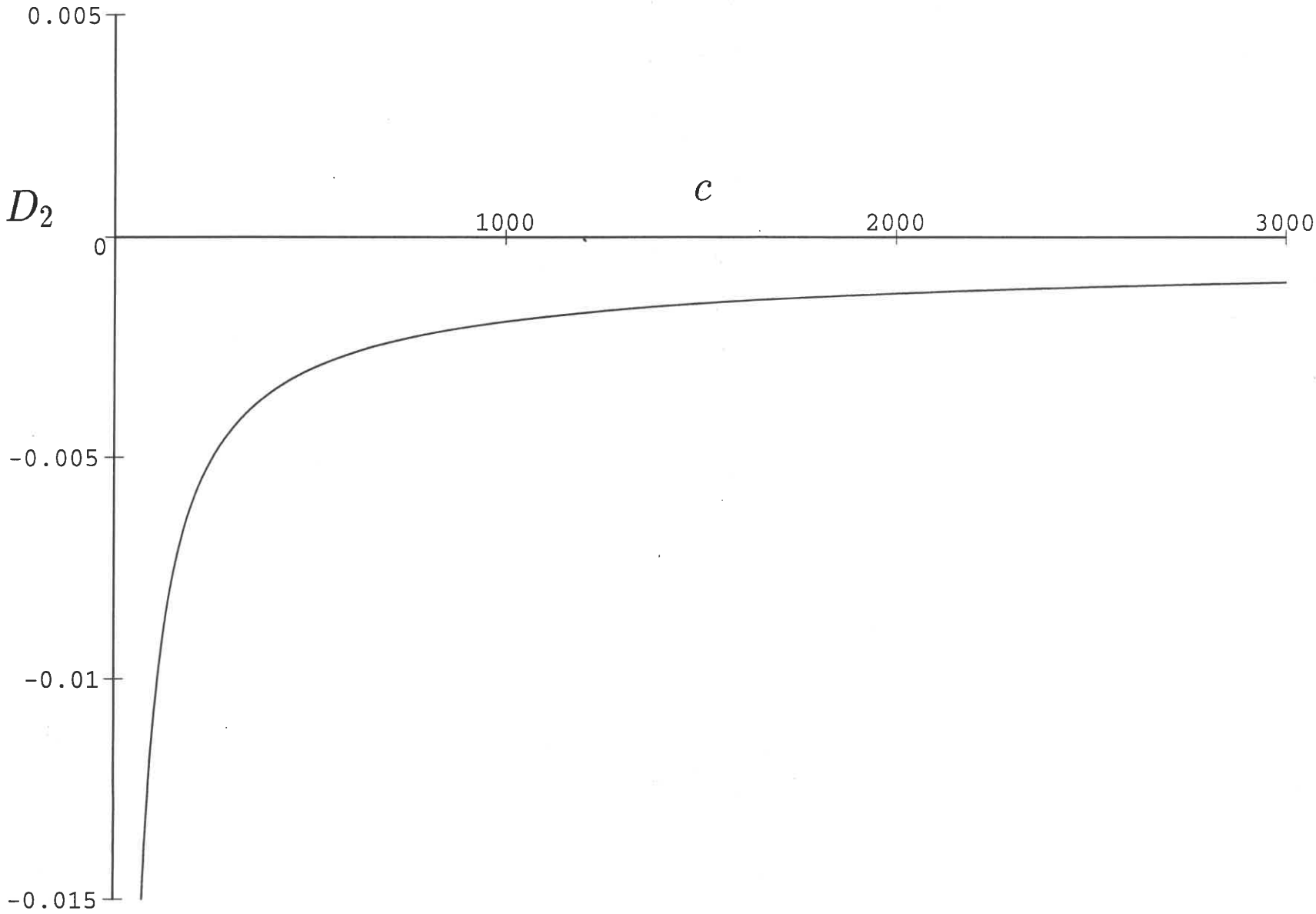

Fig. 27

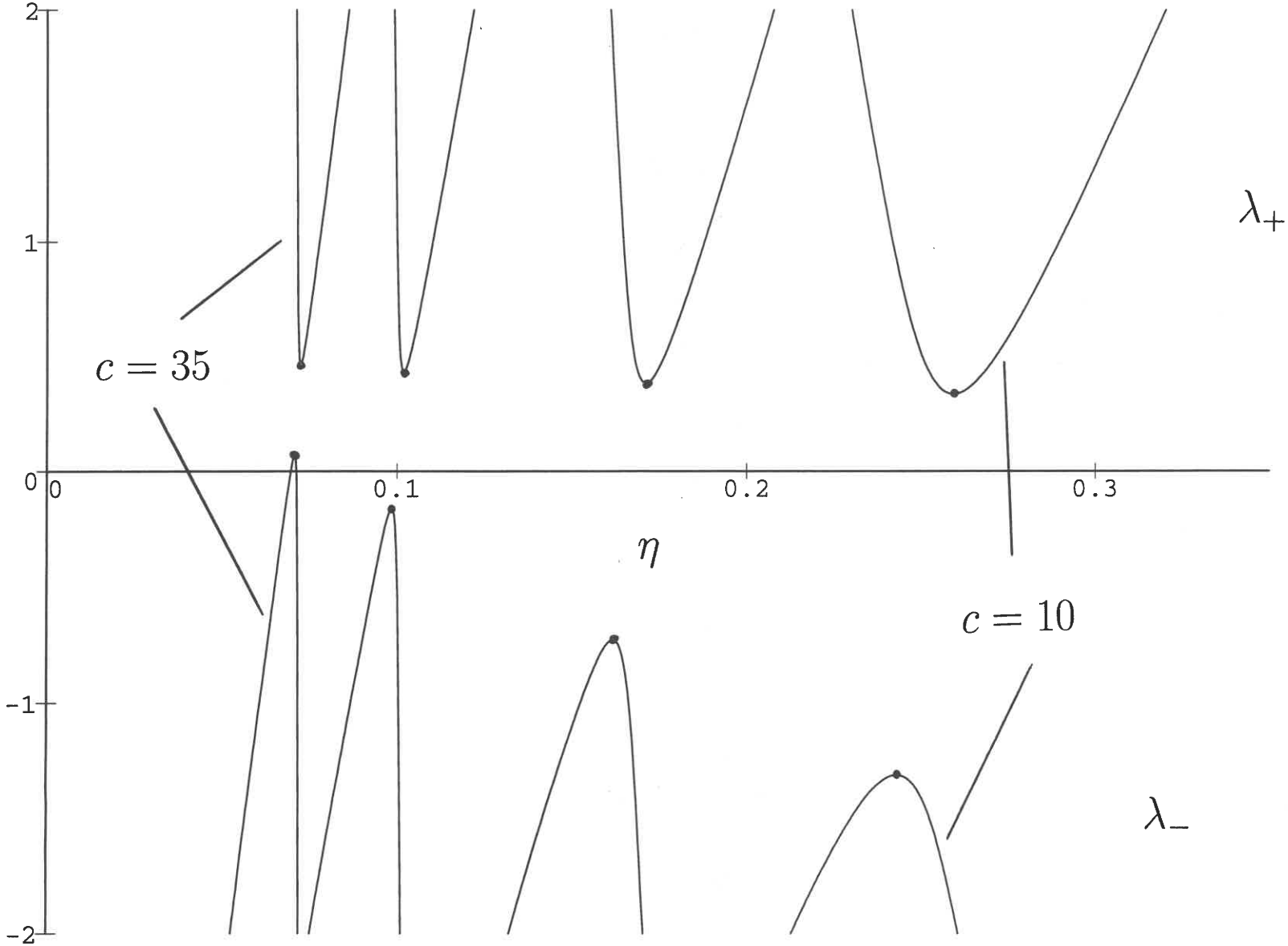

Fig. 28